Spurious Radiation Suppression in Microstrip Monopulse Antenna

Allaeldien Mohamed G. Hnesh

Submitted to the
Institute of Graduate Studies and Research
in partial fulfillment of the requirements for the degree of

Master of Science
in
Electrical and Electronic Engineering

Eastern Mediterranean University
February 2017
Gazimağusa, North Cyprus

Approval of the Institute of Graduate Studies and Research

Prof. Dr. Mustafa Tümer
Director

I certify that this thesis satisfies the requirements as a thesis for the degree of Master of Science in Electrical and Electronic Engineering.

Prof. Dr. Hasan Demirel
Chair, Department of Electrical
and Electronic Engineering

We certify that we have read this thesis and that in our opinion it is fully adequate in scope and quality as a thesis for the degree of Master of Science in Electrical and Electronic Engineering.

Asst. Prof. Dr. Rasime Uyguroğlu
Supervisor

Examining Committee

1. Prof. Dr. Hasan Demirel

2. Prof. Dr. Abdullah Öztoprak

3. Asst. Prof. Dr. Rasime Uyguroğlu

ABSTRACT

The monopulse technique has been widely used for target detection in Radar Tracking Systems. Various modern technologies have been used to implement it. The use of microstrip technology in the monopulse technique attracted a lot of researchers due to the light weight and the ability to integrate the antenna with the monopulse processing network in one structure. In most of the implementations the effect of monopulse processing network on the antenna performance is not considered. In this work, a novel shielding method is proposed to isolate the feed network form the system without loss of compactness.

The proposed method might be used in different applications however special emphasis is given to the monopulse systems. A study has been carried out using the full wave Microwave Simulation software CST to demonstrate the efficiency of the shielding method, as well as a comparison between the planer monopulse shielded system and the conventional planer system. The design frequency was chosen to be 3GHz and the commercial FR-4 substrate was used. The final designed array was further improved by using a non-rectangular distribution, to reduce the minor lobes due to the planar array nature.

The improved design exhibited difference nulls exactly at zero with depths about -23dB, the sum pattern maximum directivity was 18.4 dBi with sidelobes less than -23dB in E and H- planes. Due to the suppression of the feed network radiation the patterns of the proposed design were much more symmetrical than conventional monopulse arrays with deeper nulls.

Keywords: Monopulse antenna, microstrip arrays, spurious radiation, feed network shielding, null depth.

ÖZ

Tek darbe tekniği, Radar İzleme Sistemlerinde sinyal algılaması için yaygın olarak kullanılan bir yöntemdir. Günümüze kadar bu tekniği uygulamak için çeşitli modern teknolojiler kullanılmıştır. Bu teknik, mikro şerit teknolojisinin kullanımı, antenin tek darbe işleme ağına tek bir yapıda entegre edilmesi ve hafifliği nedeniyle bir çok araştırmacıyı cezbetmiştir. Uygulamaların çoğunda, tek darbe işleme ağının anten performansına etkisi göz önüne alınmaz. Bu çalışmada, sistemin besleme ağını yalınlaştırmak için yeni bir koruyucu yöntem önerilmektedir.

Önerilen yöntem tek darbe sistemleri için özel tasarlanmış olmasına rağmen farklı uygulamalarda da kullanılması mümkündür. Koruyucu yöntemin verimliliğini göstermek için tam dalga Mikrodalga Benzetim yazılımı (CST) kullanılarak bir çalışma gerçekleştirilmiş ve tek darbe korumalı sistem ile geleneksel düzlemsel sistem arasında karşılaştırma yapılmıştır. Tasarım frekansı 3 GHz, tasarım malzemesi de FR-4 seçilmiştir.

Son anten tasarımı, düzlemsel dizi niteliğinden dolayı meydana gelen küçük lobları azaltmak için dikdörtgen olmayan bir dağılım kullanarak daha da geliştirilmiştir. Geliştirilmiş tasarım, -23 dB'lik boşluk derinliği ile tam sıfır açısında derinlik sergilemektedir; toplam örüntü maksimuma yönelme 18.4 dBi ile E- ve H-düzlemlerinde yan loblar -23 dB'den daha azdır. Besleme ağı radyasyonunun bastırılmasından ötürü, önerilen tasarımın hüzmeleri, geleneksel tek darbe dizilerinden çok daha simetriktir ve boşluk derinliği daha fazladır.

Anahtar Kelimeler: Tek darbe anten, mikroşerit dizi, yapay radyasyon, besleme ağı yalınlaştırması, boşluk derinliği.

To my beloved parents

Dr. Halima Megei & Dr. Mohamed Hnesh

ACKNOWLEDGMENT

I would like to thank my supervisor Asst. Prof. Dr. Rasime Uyguroğlu for her patient and unlimited support through this work. As well as her contribution in forming my academic identity through the courses she gave me during my study at the EMU.

It is also a must to mention Prof. Dr. Abdullah Öztoprak, who initiated my interest in this topic and continued providing us with his valuable comments and feedback.

I am grateful as well to the department chairman Prof. Dr. Hasan Demirel for his guidance during my study period in the department.

Finally without the support of my family it wouldn't be possible to accomplish this work, all credit to them for giving me the opportunity to take this research path.

TABLE OF CONTENTS

LIST OF TABLES

LIST OF FIGURES

LIST OF SYMBOLS AND ABBREVIATIONS

EM	Electromagnetic
IEEE	Institute of Electrical and Electronics Engineers
Δ	Difference
E	Electric field intensity
$\sum$	Sum
L	Length
Y	Admittance
γ	Propagation constant
ε_r	Relative permittivity
ε_{reff}	Effective relative permittivity
h	Height
W	Width
CST	Computer simulation technology
F_r	Resonant frequency
C	Speed of light
λ_g	Wavelength of propagation
λ_0	Free space wavelength
V	Voltage
S_{ij}	Scattering matrix element
Z	Impedance
FR-4	Flame Retardant 4
TEM	Transverse electromagnetic
H	Magnetic field intensity

VSWR	Voltage standing wave ratio
3-D	Three dimensional
2-D	Two dimensional
SLL	Sidelobe level

Chapter 1

INTRODUCTION

1.1Overview

Radar or radio detection and ranging is one of the major EM (Electromagnetic) theory applications since the World War II, it started with the simple idea that is, sending EM weaves toward a region of interest and estimate information about the objectives in that region based on the reflected waves [1]. The main function of a radar system is to estimate the distance to the target and the relative angle between the system reference and the target location. Many algorithms and methods have been developed through the years to accurately specify both of those parameters.

In tracking radar, the device central axis is required to be aligned to the moving target and therefore fast position and angle detection is required. The main method for such purpose in the 40's was the lobe switching which suffered some disadvantages. However the monopulse technique come as a superb solution where, as the name indicates, unlike other techniques the monopulse requires only one pulse to estimate the angles in two coordinates [2]. The term monopulse is defined in IEEE standards [3] as "A radar technique in which information concerning the angular location of a target is obtained by comparison of signals received in two or more simultaneous antenna beams". The monopulse is referred to also as simultaneous lobing, which is despite being rarely used, is more precise where most monopulse systems usually use a raw of pulses to improve the estimation [2].

The monopulse system consist of the EM waves transceiver (the antenna), the feeding components, the patterns forming network and lastly the receiver that convert the microwave signals into an intermediate frequency for further processing [2]. Traditionally Cassegrian reflectors and waveguide components are applied to realize the system [2], however such realization result in an expensive heavy structure [4], and for tracking proposes fast movement and light weight are of high importance. The use of microstrip technology was a straightforward solution since it has the best performance in that regard. On top of that the use of the printed circuit technology allows the integration of the processing network with the antenna in a compact structure which can be single-layered or multi-layered. On the other hand such integration will affect the antenna performance, therefore integrating the pattern forming circuit with the antenna with minimum loss in performance was a determination for the researchers up until recent years.

The traditional direct way is to print the pattern forming network and the antenna on the same layer, an example of this method is the work proposed by Hao Wang et. al. [4] where they proposed 16 by 16 array printed on the same layer with the feed network. However they discussed the limitation in the performance due to the spurious radiation from the beam forming network. This effect of the feed network degrading the microstrip array performance is well known for miccrostrip researchers since the early days of this technology, where Pozar [5] listed the radiation from the feed network as one of the sidelobe sources, and discussed some possible solutions. K-L Wu [6] and others studied the effect of feed network on the antenna pattern for series fed arrays and stated its significance. A similar work but on corporate feed effect was done by [7].

Recently a lot of researchers are using multilayered structures to reduce the effect of the feeding network in microstrip array. M.T. Ali et. al. [8] separated the feed network from the radiating elements by an air gap to increase gain and reduce sidelobes. Senhang He and others [9] introduced a multilayered structure where strip lines and metal via feeds are used, however despite the improved performance problems in fabrication were reported. A similar structure proposed by Nidhees Kumar TR et. al. [10] with metal via and back to back substrate to shield the radiation pattern. Nurulazlina Ramil and others [11] used a multilayered structure with aperture coupling to reduce this spurious radiation. The success in the blockage of unwanted radiation and the complexity varies for the mentioned methods, the technique proposed in this work is quite simple and might be used in their respective applications.

The separation of the feed network and the radiating elements in different layers was used along other techniques as well to boost the performance of the planar monopulse antenna [12] [13]. The multi-layering was used for other purposes as well such as broadening the bandwidth [14] and for dual polarization [15]. Some researchers also integrated different technologies to accomplish the design, such as realizing the antenna part using the microstrips and the pattern forming part using waveguides [16] [17].

1.2Thesis Objectives

The thesis objective is to introduce a method that shields the radiation pattern of the microstrip arrays from the spurious radiation due to the feed network without loss of compactness, and to apply this method to design a planar monopulse antenna with improved performance.

1.3Thesis Contribution

The thesis propose a novel method to reduce the effect of the feeding network specifically the effect of the pattern forming network on the planer monopulse antenna. A 3GHz microstrip monopulse antenna with improved performance was designed. The proposed shielding technique can be used for other applications.

1.4Thesis Organization

In chapter 1 an overview of the topic with a quick literature review is provided, alongside an explanation of the thesis scope and organization. Chapter 2 is discussing in more details the monopulse system and it is components. Chapter 3 includes basics in microstrip technology including rectangular microstrip patch design, feeding methods and matching. Chapter 4 discusses the key concepts that led to the proposed shielding method and includes a comparison between a conventional corporate microstrip array versus a shielded microstrip array. The main work is in chapter 5 where the palaner monopulse antenna is designed and simulated with and without the shielding techniques this chapter includes the final conclusion and recommendations.

Chapter 2

MONOPULSE TECHNIQUE

2.1 Tracking Radar

The basic motivation for a high accuracy angle estimation in radar systems was the tracking branch. Tracking requires a real time estimation of an error signal that will direct the main axis of the antenna (called boresight) to the specific target angle [18]. Researchers were keen to develop fast and efficient algorithms for such purpose. The main methods that proved their effectiveness were the sequential lobing and the simultaneous lobing (or the monopulse technique). The monopulse is mainly an evolution of the sequential lobing to overcome its limitations.

In sequential lobing the antenna single main beam is successively displaced mechanically or electrically, with pulse transmission and echo measurements done each time. The sequential scanning can be realized by a single antenna with the proper displacement mechanism, and it is shown in figure 2.1.

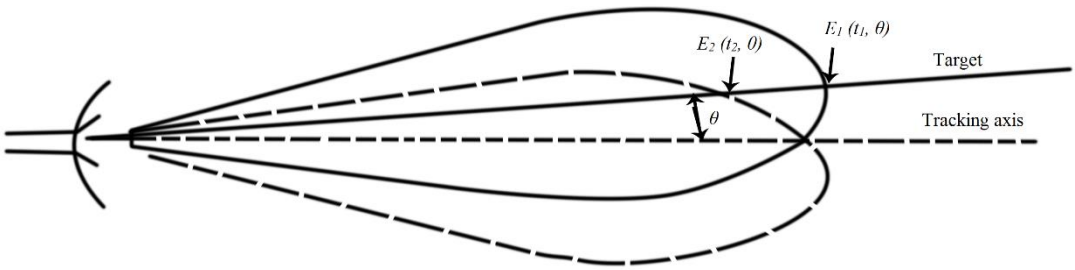

Figure 2.1: Sequential lobing

The difference signal is then generated:

$$\Delta = E_1(t_1, \theta) - E_2(t_2, \theta) \tag{2.1}$$

The magnitude of the difference function indicates the magnitude difference between the target relative angle to the boresight axis, and the sign will indicate the direction in the scanning plane (i.e. if the relative angle is positive or negative). Figure 2.2 shows two examples of sequential lobing where (A) and (B) are successive positions for the antenna beam [19].

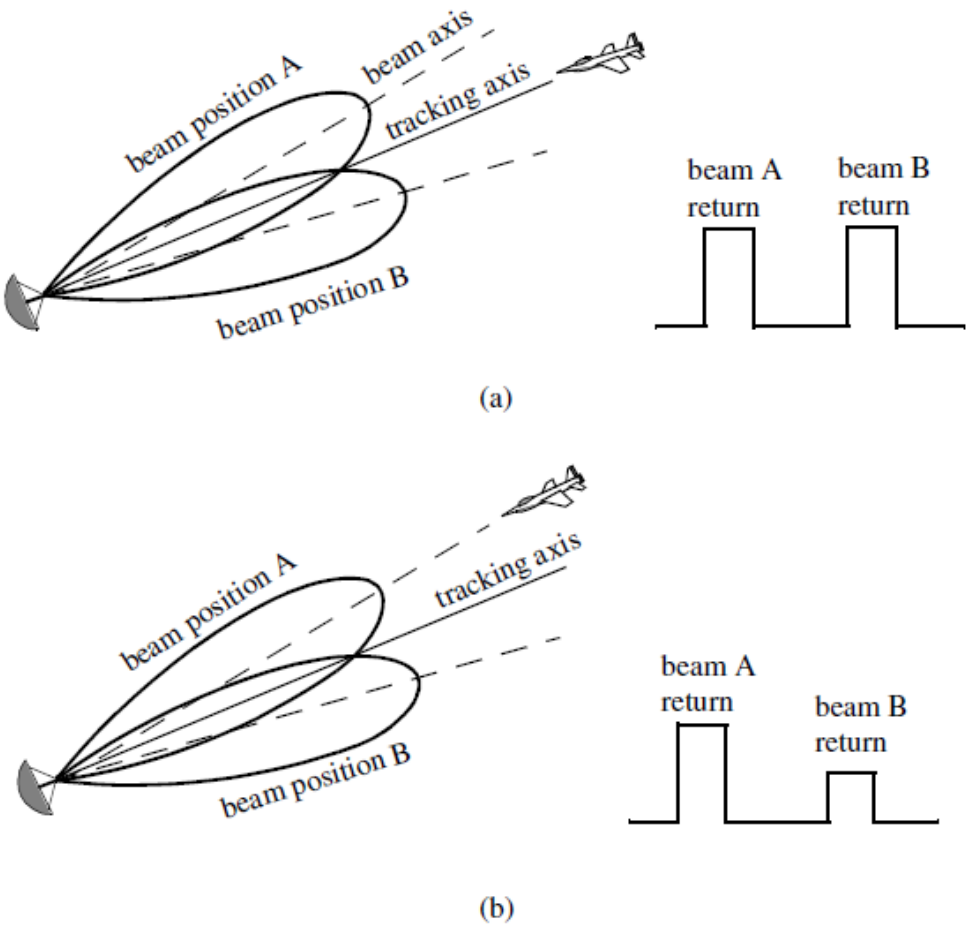

Figure 2.2: Sequential switching demonstration [19]

Because the sequential lobing is time dependent errors may occur with target signal amplitude variation with time [18]. Errors also occur as a result of mechanical

vibration [2] and some jamming techniques are effective against such a technique [1]. A similar concept type is the canonical scanning, for more details one may refer to the references.

2.2 Simultaneous Lobe Comparison (monopulse)

Instead of the successive change of a single beam proposed by sequential switching, the monopulse technique suggests a simultaneous generation of multiple beams at a time [19]. Generation of two beams at a time can be realized by using more than one element, a microwave network is then used to generate correction signals known as the sum and the difference patterns. Figure 2.3 shows the simultaneous lobing method.

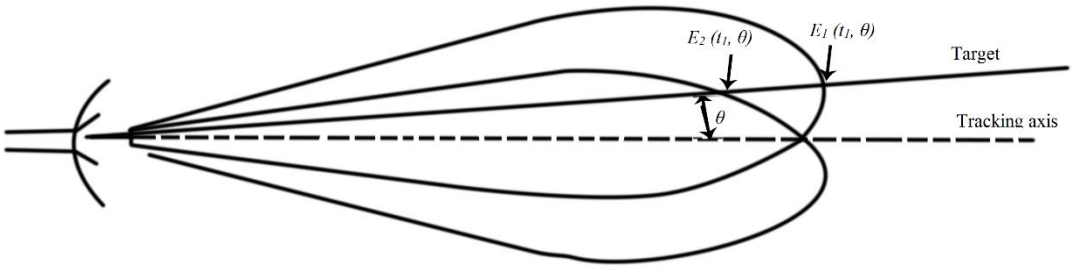

Figure 2.3: Simultaneous lobing

In addition to the difference signal similar to the one in equation 2.1, the sum signal is generated as well:

$$\sum = E_1(t_1, \theta) + E_2(t_1, \theta) \tag{2.2}$$

According to the type of the processing amplitude or phase difference or a combination of both might be used to determine the angular error signals [2]. Figure 2.4 shows the sum and difference patterns. For complete angle detection in both of the orthogonal coordinates the process is done in both azimuth and elevation planes. Figure 2.5 shows a three dimensional monopulse pattern.

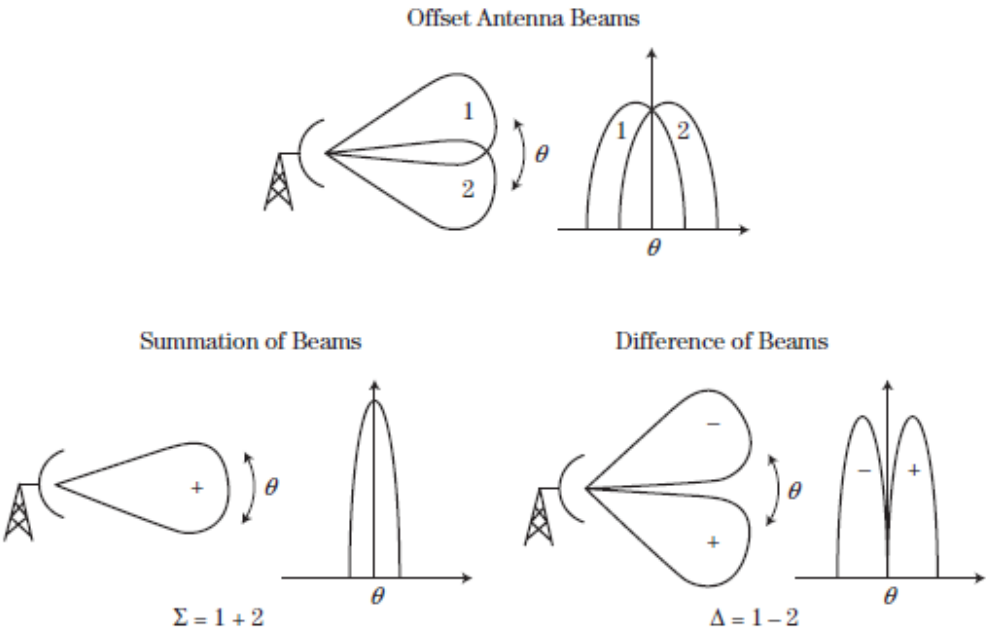

Figure 2.4: The monopulse sum and difference patterns [1]

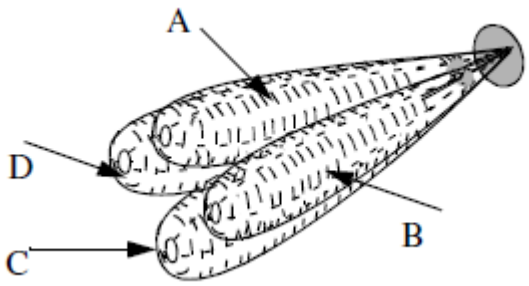

Figure 2.5: 3- D monpulse patterns [19]

The monpulse technique hence need only one pulse to estimate the target angles which makes it faster than the sequential scanning, as well as being non-vulnerable to errors due to echo fluctuation with time and errors due to mechanical vibration. Due to these and other factors, the monopulse technique achieves lower sidelobes than the sequential lobing [18].

2.3 Monopulse System

The monopulse system in general is divided into two parts. A transceiver responsible for transmitting the test pulse and forming the sum and difference patterns while receiving the echo simultaneously and a processor that will extract the information about the angular location. In tracking radar this information will be used later to realign the antenna boresight to the target [1].

A simplified diagram for the amplitude monopulse technique is shown in figure 2.6. Four antennas (each antenna might be in the form of subarray) are used to form 4 distinct patterns. Usually reflector antennas, horns and lens antennas are used for this porpuse [2]. However for applications where light weight is required, microstrip antenna arrays have achieved very good performances.

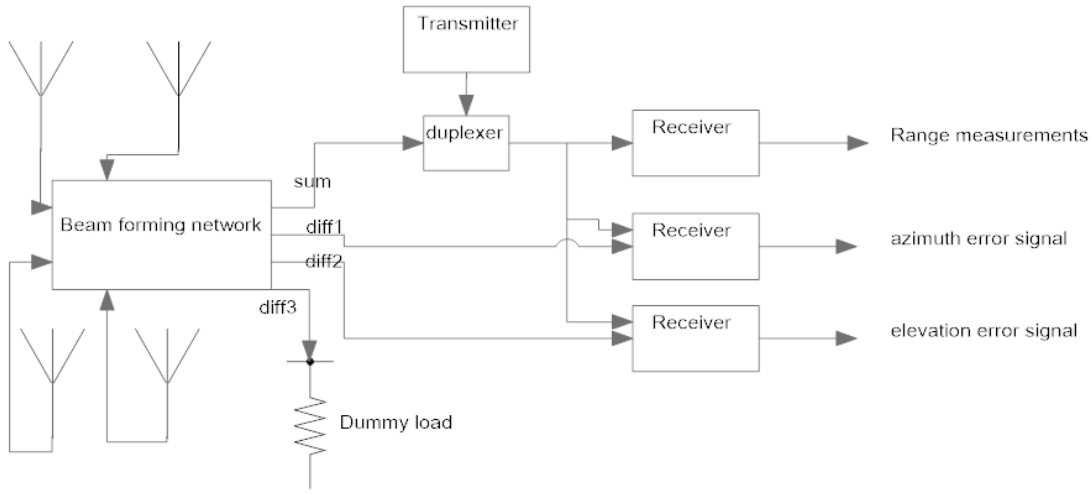

Figure 2.6: Monopulse system block diagram

A microwave network is used to form the monopulse sum and difference patterns, this network might be realized by different microwave elements. A possible way is to construct it using the 180^0 hybrids [2]. Another way is to use the quadrature hybrids as shown in figure 2.7, and this method is used later in the realization of our design.

The beam forming network will result in a sum of the elements patterns, the difference in azimuth plane, the difference in elevation plane and the difference in the diagonal plane which will not be used and will be terminated with a matched load.

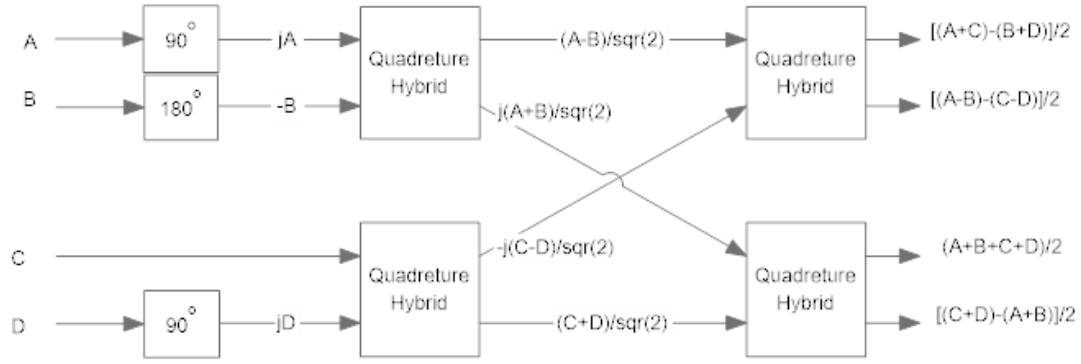

Figure 2.7: The beam forming network for four patterns A, B, C and D

The sum port might be used for transmission as well as receiving, and therefore a duplexer (can be realized by a microwave circulator) is used. The sum port is used for range measurements and to provide a phase reference for other ports [19]. Finally before processing the received echo the microwave signals should be transformed to an intermediate frequency. This is done by the receiver as shown in figure 2.8. The angle error signals in both coordinates will indicate the deviation of the boresight of the beams from the target.

Since Δ in equation 2.1 is a function of the range and the angular position, it is better for the difference receivers to use the ratio of the difference to the sum $\left|\frac{\Delta}{\Sigma}\right|$ rather than the difference signal to get more accurate estimate for the angular location [19].

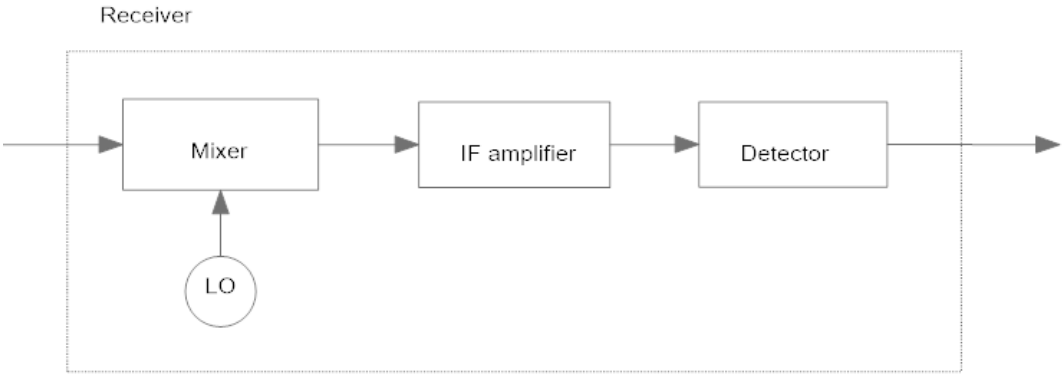

Figure 2.8: Receiver components

2.4 Monopulse Patterns Characteristics

In this work our aim is to design the monopulse antenna for the previously mentioned system integrated with the beamforming network. The rest of the system is not in the scope of this thesis. In this section we will model the ideal sum and difference beams and define some of their basic characteristics in order to be able to judge any monopulse antenna design.

A conventional way to model the pattern of an antenna is to use the sinc function [2] [19]. Limiting our discussion to one plane at a time we can model the patterns A and B with the following equation respectively:

$$E_A = \frac{\sin(\theta-\theta_o)}{(\theta-\theta_o)} \tag{2.4}$$

$$E_B = \frac{\sin(\theta+\theta_o)}{(\theta+\theta_o)} \tag{2.5}$$

Figure 2.8 shows those patterns where they represent two identical patterns separated by the optimum distance for the best performance of the two element array. For the demonstration purposes the shift angle is chosen arbitrary. Figure 2.9 shows ideal sum and difference patterns.

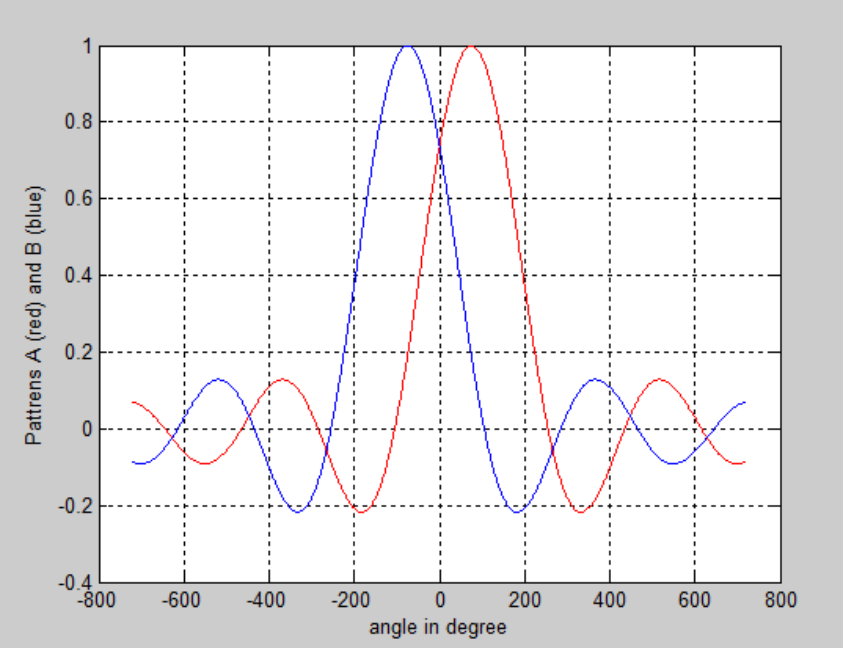

Figure 2.9: Two distinct patterns for the two elements array of the monpulse antenna

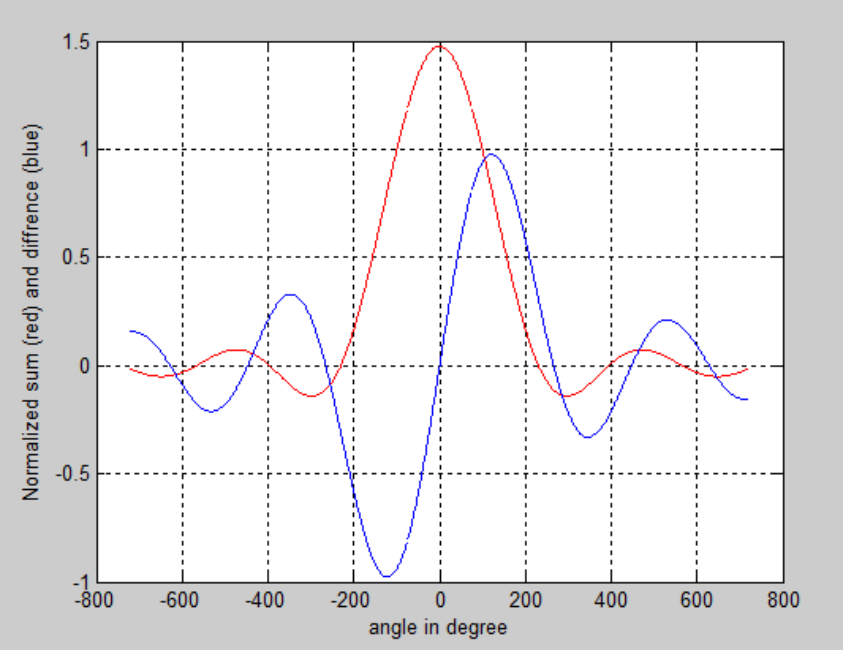

Figure 2.10: Ideal sum and difference patterns

From figure 2.9 we can see that an ideal monopulse antenna has a sum pattern with a maximum at the antenna center (0^0) and a zero difference at the same point. Usually such patterns are represented in decibels as shown in figure 2.11. Due to the perfect

symmetry all nulls in figure 2.11are infinitely negative. To sum up two basic characteristics are critical in the design of a monopulse patterns:

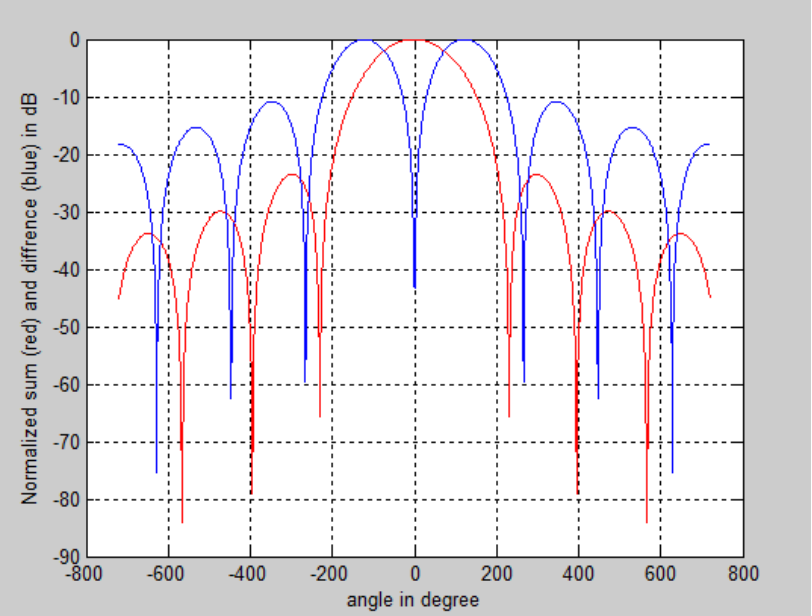

Figure 2.11: Ideal sum and difference patterns in dB

1. **The Null depth**: This is a property of the difference pattern and it indicates how symmetric the monopulse patterns are. Ideally it is zero at the structure center (0^0) or negatively infinite in dBs However in practical design due to various limitation the null is deviated from the center and it has a non-infinite value.

2. **Sidelobes**: this is a property of both sum and difference pattern, and it is specifically vital for the sum pattern since it is used as a reference and for transmission as well. The sidelobe according to the IEEE standard definitions is [20] "A radiation lobe in any direction other than that of the major lobe". As seen from figure 2.11 sidelobes exist even in the ideal case due to the nature of the beams. However minimizing sidelobe is vital in all antenna applications.

Chapter 3

MICROSTRIP TECHNOLOGY

3.1 Printed circuits and Microstrip Antennas

Printed circuits technology has been the most popular choice when it comes to mass production for the various electrical and electronics applications, they provide a fast and low cost approach to fabricate various devices. The microstrip technology is classified as a printed circuit technology, sometimes the microstrip antenna is even called the printed antenna [21]. Actually the studies of the unwanted radiation in the printed thin strip line circuits triggered the idea of trying to guide such a radiation and making use of it, and that was the birth of the idea in the 1950's [22]. However the first practical antenna was designed and fabricated 20 years later [21], [23]. Since then the motivation of having such a low profile, low cost antenna was the basic drive for years of research to meet the new demands of modern life devices.

The microstrip antenna consist of a metallic ground below a dielectric substrate as shown in figure 3.1. Above the substrate there is a metallic radiator called the patch, which can take various shapes. The shape of the radiator is usually chosen to be familiar in order to simplify the analytical part in order to predict the antenna performance [21]. Some examples of the patch shape can be seen in figure 3.2.

Beside its low profile the microstrip antenna has the vital property of being integrable with other printed circuits. This is important for applications where the beam forming

network is required to be integrated such as monopulse antenna, which we will implement using microstrip technology. The microstrip antenna covers as well a wide range of frequencies approximately from 100MHz to 100GHz [21].

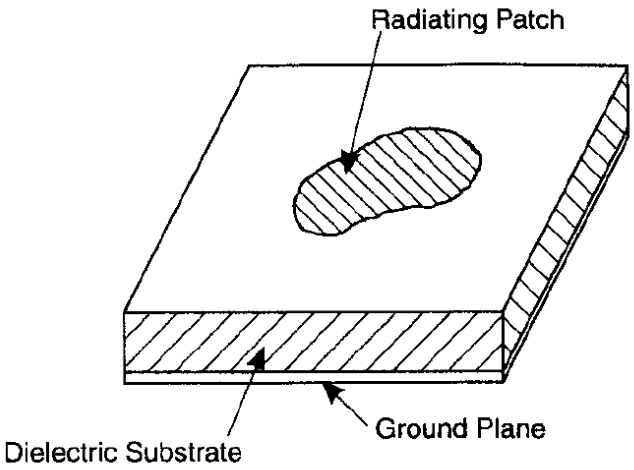

Figure 3.1: Microstrip antenna basic structure [21]

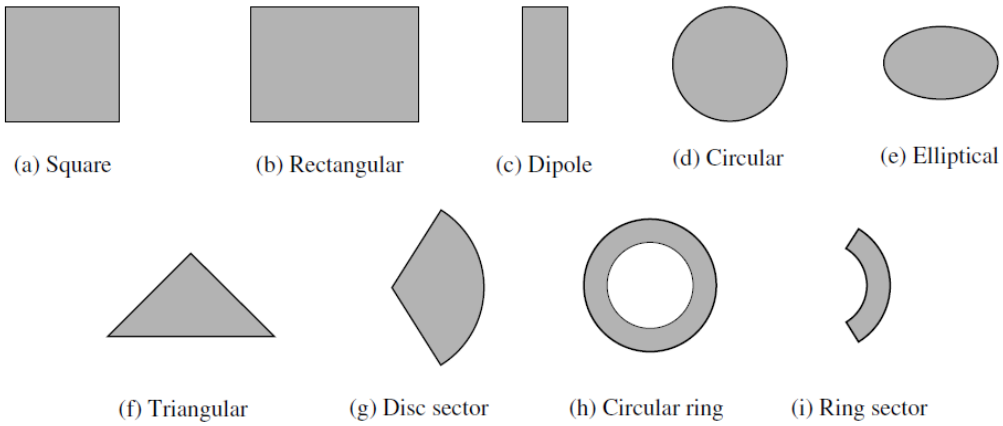

Figure 3.2: Examples of patch shapes [23]

However the microstrip antenna suffers from major disadvantages such as its high and various losses resulting in relatively low efficiency compared to other antennas, as well as a smaller bandwidth and lower gain. Most microstrips radiate into half space

only [21]. The major disadvantage related to our topic is the superior radiation from the feed lines that has been mentioned in [22] and [23].

The flow diagram shown in figure 3.3 must be followed in order to successfully deploy the microstrip antenna and integrate it to the system. This includes the choice and design of the antenna patch, the feeding method and the matching network to couple the energy properly to the rest of the system.

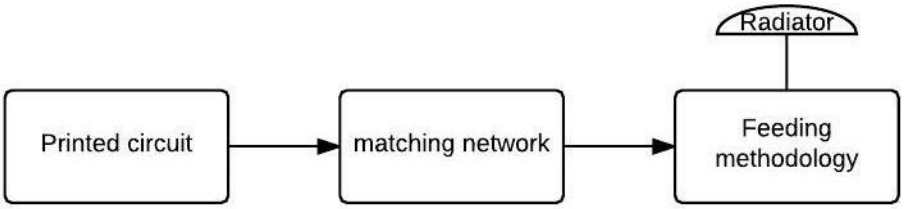

Figure 3.3: Microstrip antenna design general diagram

3.2 Microstrip Antenna Feeding Methodologies

Feeding is the way of coupling the energy to the radiator. The variety of feeding methods gives a broader options to the designers to meet the system requirements. The microstrip antenna can be fed by a coaxial cable, a microstrip line or even a strip line as we propose in this work. The probe coupling by a coaxial line for a circular patch is shown in figure 3.4. Feeding with microstrip line can be divided mainly to co-planar feeding, where the patch and the line are on the same layer, and coupling when the line is on another layer.

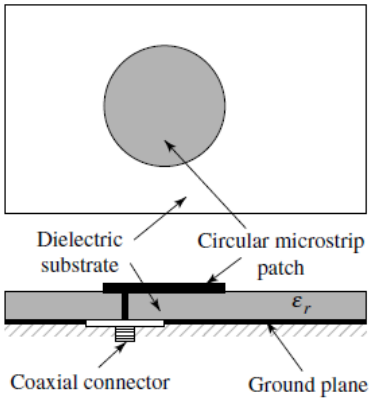

Figure 3.4: Probe feed for a circular patch [23]

Coplanar coupling can be a gap coupling or a direct coupling as shown in figure 3.5. For application where the feed line is on a different layer there is aperture coupling which is the most difficult feed technique to model but it has the lowest spurious radiation [23], and the proximity coupling method which has the advantage of the broad bandwidth. Both aperture coupling and proximity coupling are shown in figures 3.6 and 3.7 respectively.

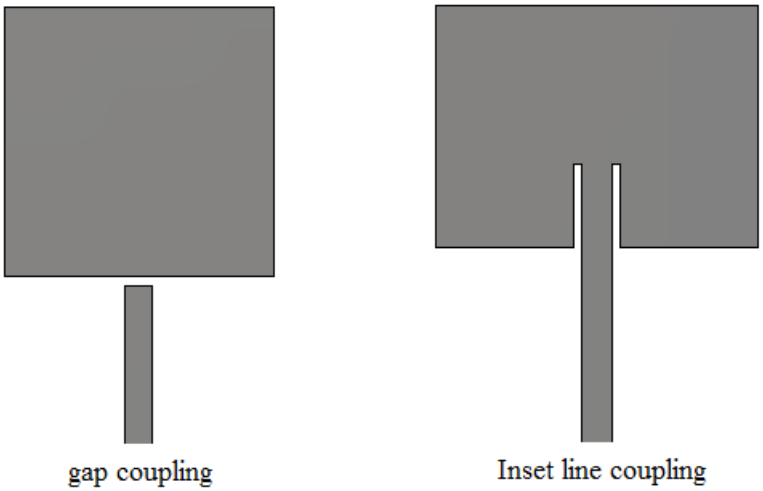

Figure 3.5: Coplanar microstrip patch coupling

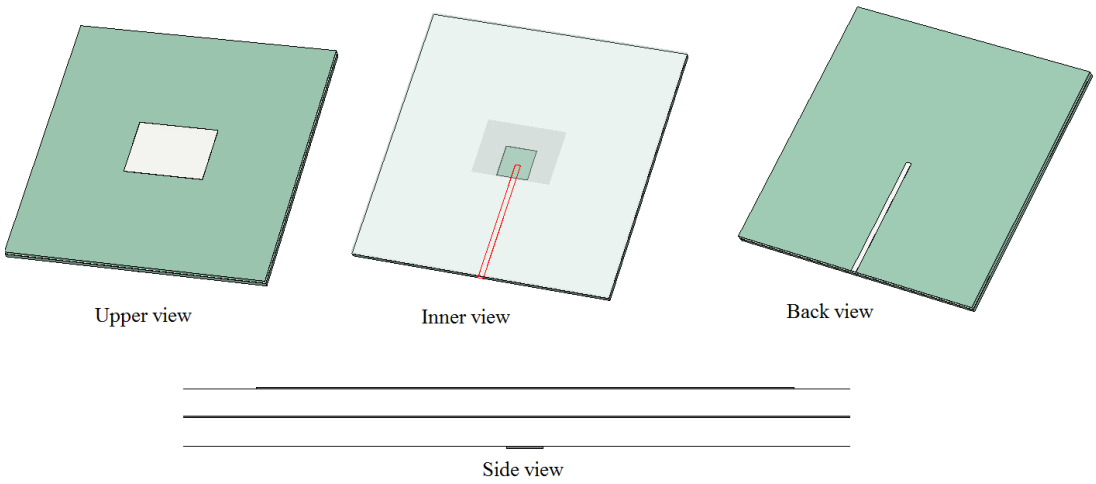

Figure 3.6: Aperture coupling

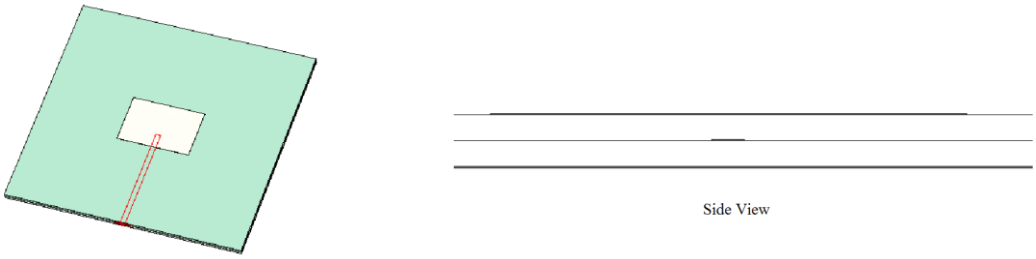

Figure 3.7: Proximity coupling

3.3 Rectangular Microstrip Design and Matching

The rectangular shape is the most widely used and analyzed patch type and it will be used through the thesis work therefore special emphasis will be paid to it. In general to analyze the patch antenna the most accurate method is the full wave analysis that includes solving the integral equations. However popular methods of representing the patch with a known structure such as the transmission line model and the cavity methods are pretty popular, they simplify the analysis and give a better physical insight [23]. Fortunately today despite the error in such models, with the software tools available, starting by a simple model and then optimizing it saves a lot of time rather than the complex analysis path.

Transmission line model for instant represents the antenna by two slots connected through a transmission line of a length equal to the patch length [23]. Figure 3.8 shows the transmission model for a rectangular microstrip patch with a probe feed. The probe divided the patch into two lines of lengths L_1 and L_2 with a characteristic admittance of y_c, a propagation constant γ, and two terminations y_s representing the open end terminations [21].

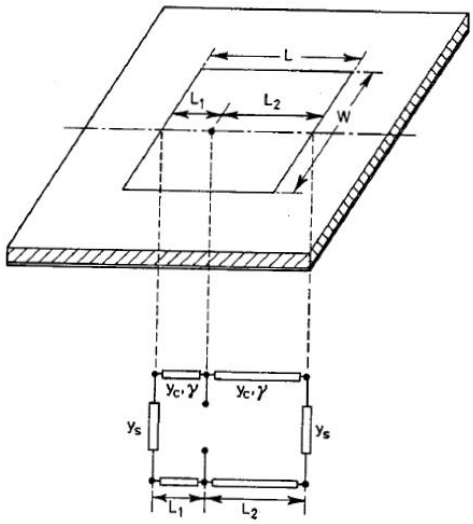

Figure 3.8: Transmission line model for a rectangular patch antenna with probe feed [21]

However the model accounts for the fringing effect that makes the antenna electrical length greater than its actual length. As well as introducing the effective permittivity to model the wave propagation in both the air and the dielectric substrate. The fringing effect is shown in figure 3.9. The antenna effective permittivity concept is shown in figure 3.10, and the antenna electrical effective length is shown in figure 3.11.

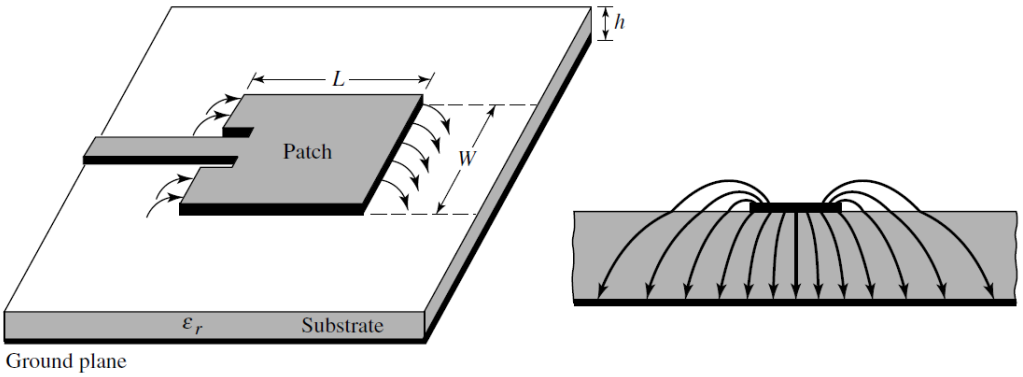

Figure 3.9: Fringing effect in microstrip patch antenna [23]

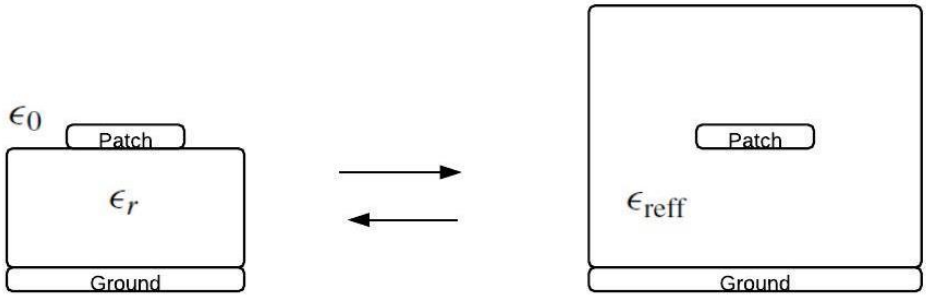

Figure 3.10: Concept of effective permittivity

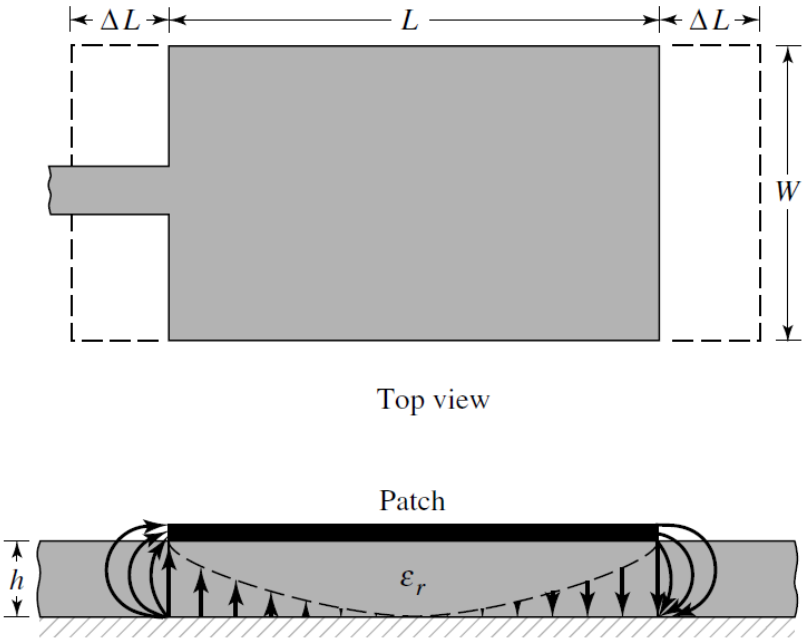

Figure 3.11: Rectangular patch antenna effective length [23]

Various approximation for the effective permittivity and effective length might be found in the open literature, however we will use the one collected by [23]:

$$\varepsilon_{reff} = \frac{\varepsilon_r+1}{2} + \frac{\varepsilon_r-1}{2}\left[1 + 12\frac{h}{W}\right]^{-\frac{1}{2}} \tag{3.1}$$

$$\frac{\Delta L}{h} = 0.412\frac{(\varepsilon_{reff}+0.3)\left(\frac{W}{h}+0.264\right)}{(\varepsilon_{reff}-0.258)\left(\frac{W}{h}+0.8\right)} \tag{3.2}$$

$$L_{eff} = L + \Delta L \tag{3.3}$$

The design procedures in this thesis combine the use of the transmission line model with the use of the CST microwave studio software for the optimization purpose to overcome the error due to the model approximation. The diagram in figure 3.12 shows how this combination work to result in the desired patch width W and length L.

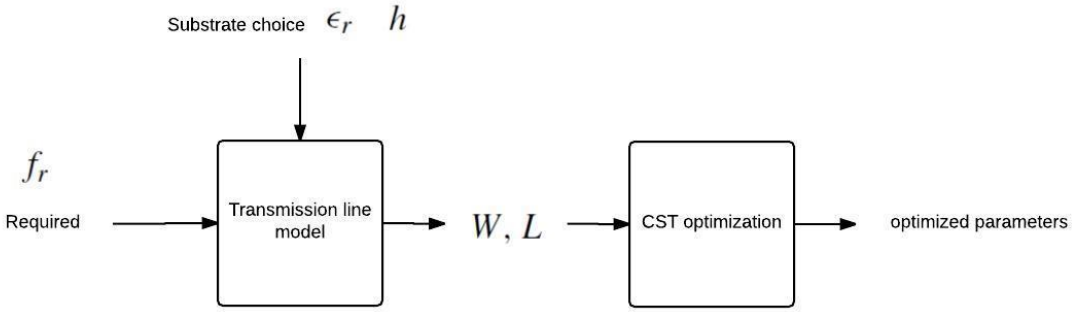

Figure 3.12: Design procedure for the rectangular microstrip patch

After a proper choice of the substrate and the working frequency according to the application, the transmission line based calculations are as follows [23]:

1- Find W:

$$W = \frac{c}{2f_r}\sqrt{\frac{2}{\varepsilon_r+1}} \tag{3.4}$$

2- Determine the effective permittivity ε_{reff} and the difference between the actual and effective lengths ΔL using equations 3.2, 3.3 respectively.

3- The actual length is then calculated by:

$$L = \frac{c}{2f_r\sqrt{\varepsilon_{reff}}} - 2\Delta L \qquad (3.5)$$

The last step is to match the patch to the feed line. Feed lines usually have a standard characteristic impedance of 50 ohm, and to minimize the reflection loss in the system the antenna input impedance should be calibrated to be near this value. This process can be done through a matching network, or a slight change in the antenna geometry in a way that changes the impedance without affecting the radiation properties.

Various matching methods are used depending on the feeding type, for coplanar fed patch antennas for example, matching might be done by the inset line method, the quarter wave length transform, or even the non-radiating edge method as shown in figure 3.13 (a), (b) and (c) respectively [22].

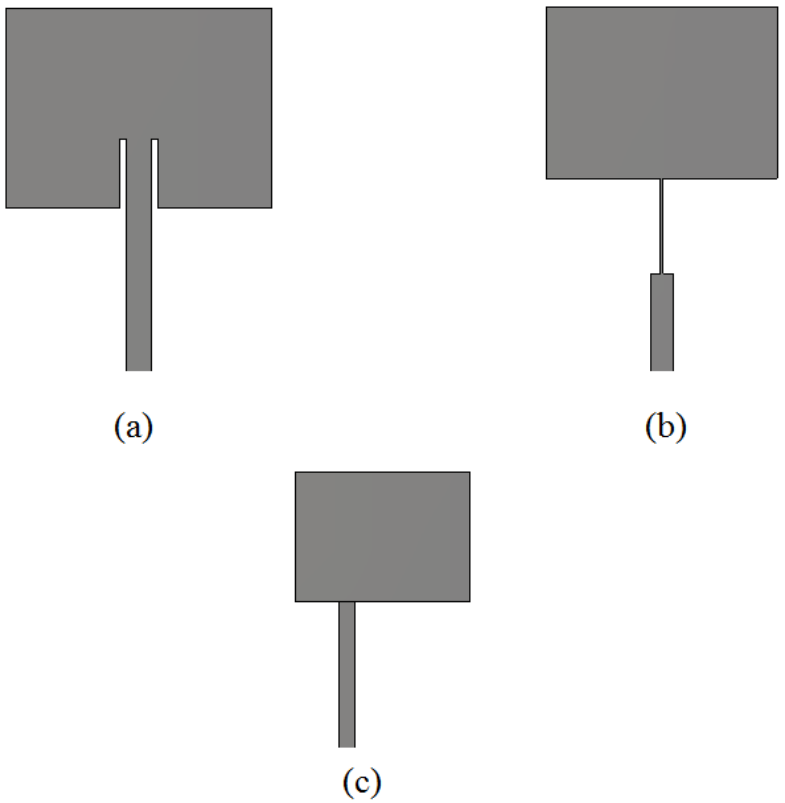

Figure 3.13: Coplanar patch antenna matching methods

3.4 Microstrip Lines

The microstrip line is one of the two conductor transmission systems which gained a great popularity with the numerous use of the microstrip technology. It is easily fabricated and integrated with other microwave devices. Figure 3.14 shows the microstrip line and the distribution of the fields during transmission.

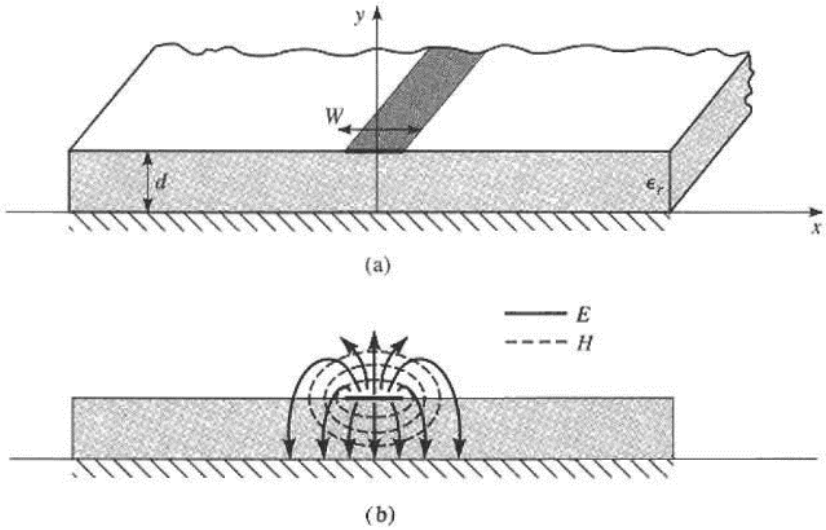

Figure 3.14: The microstrip line and the field's distribution [24]

During our work we will use microstrip lines to construct couplers, power dividers and to properly feed the antenna or the array. Two properties are vital in that regard, firstly the wavelength of propagation inside the line and its characteristic impedance. For a certain substrate to obtain the various characteristic impedances required in the different structures, the width of the strip is changed. In modeling the microstrip lines' behavior, similarly to the microstrip antennas, the concept of effective permittivity is used. A good approximation for the wavelength of propagation inside the line λ_g is given by [24]:

$$\lambda_g = \frac{\lambda_0}{\sqrt{\varepsilon_{reff}}} \tag{3.6}$$

Where λ_0 is the wavelength of the wave in free space, and ε_{reff} is effective permittivity given by equation 3.1. Various approximations for the characteristic impedance Z_c and for the synthesis of the width for a specific impedance might be found in [24-25].

The microstrip lines suffer losses due to the dielectric and conductor conductivities, in addition to that there is a radiation loss which especially arises at discontinuities such as open and short circuit terminations and bends [26]. Thicker substrates are more subject to radiation loss than thinner once [27].

3.5 Microstrip Couplers and Power Dividers

Using the microstrip lines as a realization for the transmission lines means that the microstrip technology can be used to implement different microwave components such as couplers, filters and amplifiers. The analysis of a microwave device is slightly different than the low frequency well known circuit theory where wavelength becomes comparable to the circuit dimension [24]. The best way to model a microwave device is its scattering matrix, which defines the device function as a block [25]. For a two port network as shown in figure 3.15 the scattering matrix is defined as follows [24]:

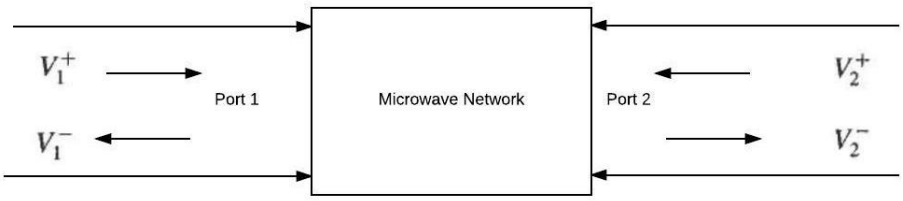

Figure 3.15: Two port microwave network

$$\begin{bmatrix} V_1^- \\ V_2^- \end{bmatrix} = \begin{bmatrix} S_{11} & S_{12} \\ S_{21} & S_{22} \end{bmatrix} \begin{bmatrix} V_1^+ \\ V_2^+ \end{bmatrix} \tag{3.7}$$

Where in general:

$$S_{ij} = \frac{V_i^-}{V_j^+}\Big|_{V_k=0\ for\ k\neq j} \tag{3.8}$$

We will discuss power dividers and the branch line couplers since they are related to the thesis topic:

1- Microstrip power divider: In this device one port is dedicated for the input signal and the device divide the power to the rest of the ports, that can be two or more, with an equal or arbitrary ratio. Later in this work we will use the T-junction which has two inputs and we will divide the power equally. In terms of the scattering matrix this device can be represented as following:

$$S = \frac{1}{2}\begin{bmatrix} 0 & 1 & 1 \\ 1 & 0 & 1 \\ 1 & 1 & 0 \end{bmatrix} \tag{3.9}$$

Various microstrip configurations can be used for such propose, two examples are shown in figure 3.16, also unequal split is possible as shown in figure 3.17. The little triangular cut in the middle point is used to make the discontinuity smoother and reduce the unwanted radiation.

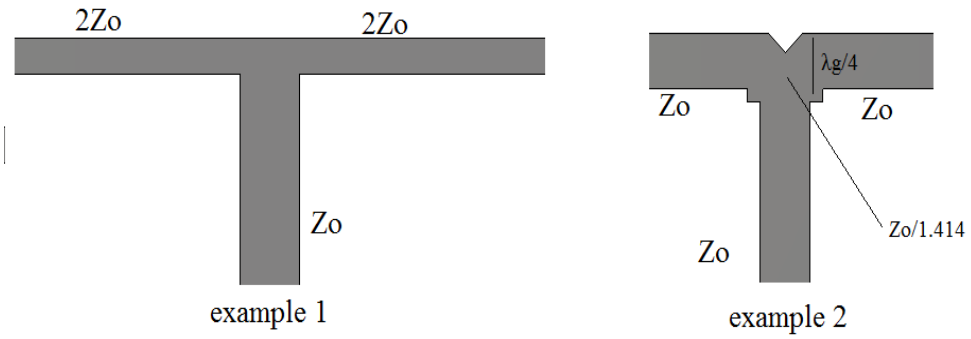

Figure 3.16: Microstrip equal power dividers

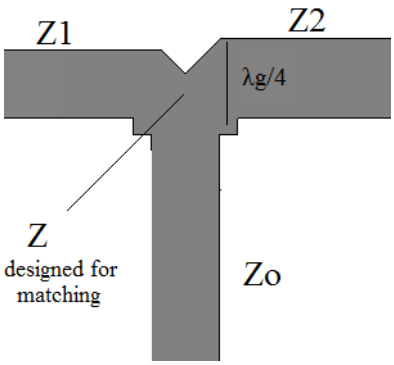

Figure 3.17: Microstrip unequal power divider

2- Microstrip hybrid line coupler: it is a four ports device that simulate the function of a hybrid coil transformer shown in figure 3.18. Under the proper matching conditions, the signal that enters port 1 will be split into ports 2 and 3 with equal phase with port 4 isolated, however if it enters port four it will be split into ports 2 and 3 out of phase with port 1 isolated [25]. In general the power division ratio can be designed to be arbitrary and the phase shift can be designed to be either 90 or 180 degrees [24]. However in microstrip couplers the limitations in the characteristic impedance realization limits the coupling factor to 2-9 dB's [25].

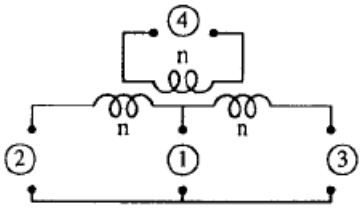

Figure 3.18: Hybrid coil transformer [25]

Figure 3.19 show a 90 degree shift hybrid coupler with arbitrary splitting ratio according to the used impedances. Later in our work we will use a quadrature

3-dB branch line coupler to construct a comparator circuit, which has the scattering matrix of equation 3.10.

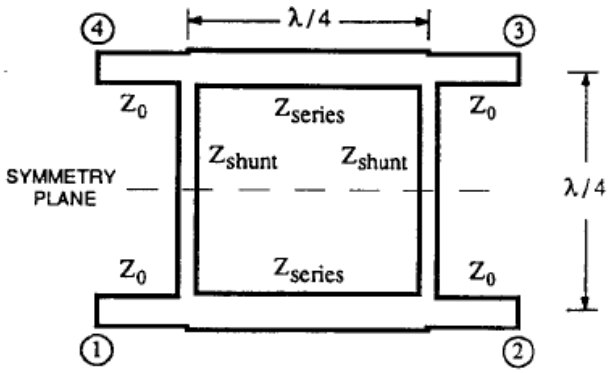

Figure 3.19: 90^0 Hybrid microstrip coupler [25]

$$S = \frac{-1}{\sqrt{2}}\begin{bmatrix} 0 & j & 1 & 0 \\ j & 0 & 0 & 1 \\ 1 & 0 & 0 & j \\ 0 & 1 & j & 0 \end{bmatrix} \tag{3.10}$$

For such a division in figure 3.19, the impedances have the following values [24]:

$$Z_{series} = \frac{Z_o}{\sqrt{2}} \tag{3.11}$$

$$Z_{shunt} = Z_o \tag{3.12}$$

The hybrid lines usually suffer from a narrow bandwidth due to the high dependency on λ_g in device operation, however slightly broader bandwidth might be achieved by using multiple sections [25].

3.6 Microstrip Antenna Arrays

As known from the antenna theory an identical number of antennas may form an array in order to synthesize a required pattern that is not possible to achieve using a single element [23]. Arrays can also be used to obtain higher gain and for beam scanning purposes. Arrays can be classified to linear arrays where all elements lie on a single

line, planer arrays where elements are placed on one plane, or even a volume array in three dimensions [21]. Various properties might be tuned to get different patterns, such as the elements distribution, the elements spacing, the amplitude and the phase differences at each antenna. Figure 3.20 shows a linear and a planar arrays of microstrip antennas respectively.

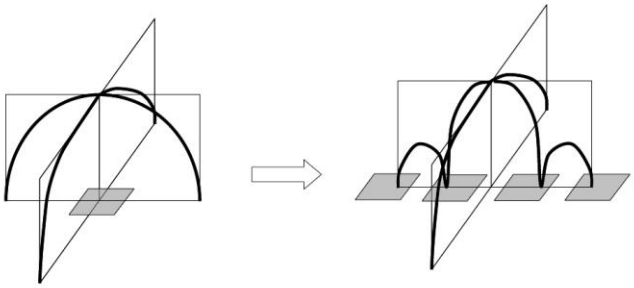

(a) Linear array

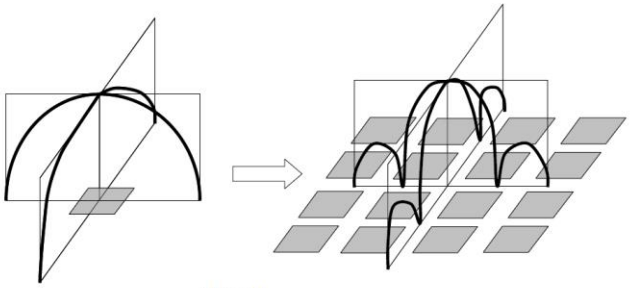

(b) Planar array

Figure 3.20: Microstrip linear and planar arrays [28]

The choice of the feeding methodology is also of high importance. There are two categories: the series feed configuration where all patches are fed by the same line, and the corporate feed configuration where the elements are fed via multiple lines descends from one line with the proper power division using power divider discussed in the previous section. Figure 3.21 shows both feeding categories for a linear microstrip array. It is also important to choose the elements separation such that the mutual coupling between the radiators and between the radiator and the feeding network is minimized [21].

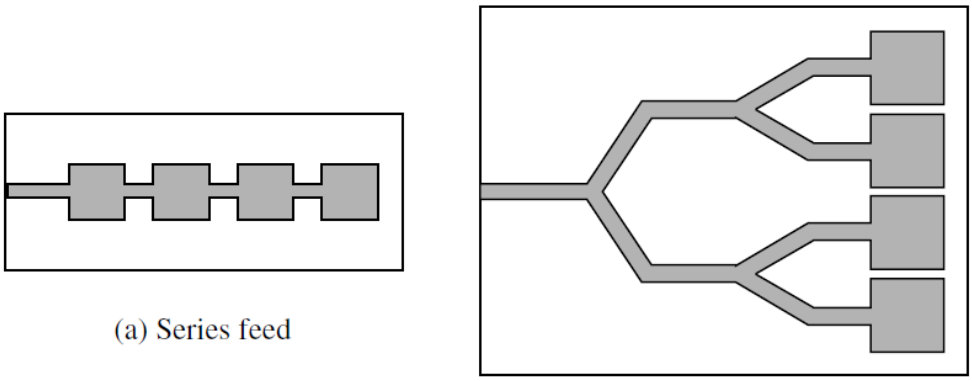

(a) Series feed

(b) Corporate feed

Figure 3.21: Series and corporate feeds for a linear microstrip array [23]

Chapter 4

THE PROPOSED SHIELDING METHOD

4.1 Radiation Loss in Microstrip Lines: An Experiment

It is mentioned in the previous chapter that one of the losses in the microstrip line is the radiation loss that specially occur at the edges and discontinuities. In the case of microstrip networks that integrate antennas with feed lines and microstrip devices (i.e. filters, couplers …) this loss will not only degrade the signal during transmission, but it will also disturb the pattern of the integrated antenna. The amount of effect varies according to the substrate type and thickness as well as the complexity of the structure.

In order to model and visualize such an effect a 50 ohm microstrip of a finite length printed on FR-4 substrate is considered. Signal transmission through the line at a frequency of 3GHz was simulated using CST microwave studio. The line is shown in figure 4.1 along longitudinal animation of the magnitude of the electric field.

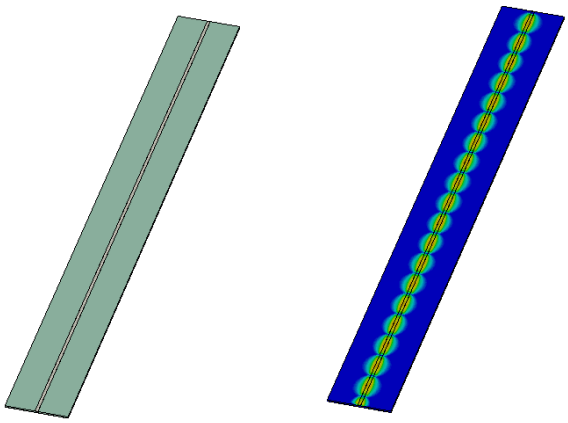

Figure 4.1: Microstrip line and the longitudinal E-field distrinution

However to get more insight a vertical cross-section perpendicular to the plane of propagation is considered in figure 4.2, the simulations are as expected in figure 3.14.

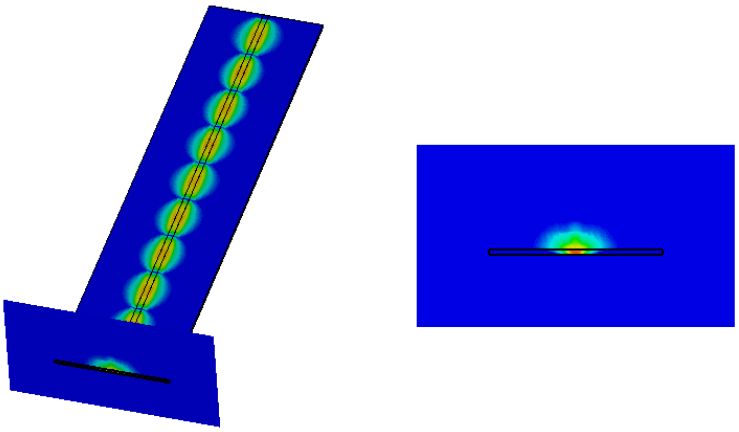

Figure 4.2: E-Field distribution in the plane of propagation for a microstrip line

In order to observe the radiation loss in the line a far field monitor around the line in the software has been set and the radiated power were observed. Figure 4.3 shows a 3-D far field pattern along the 2-D far field pattern of the directivity in the propagation plane (ϕ=0) that confirms the theory in section 3.4.

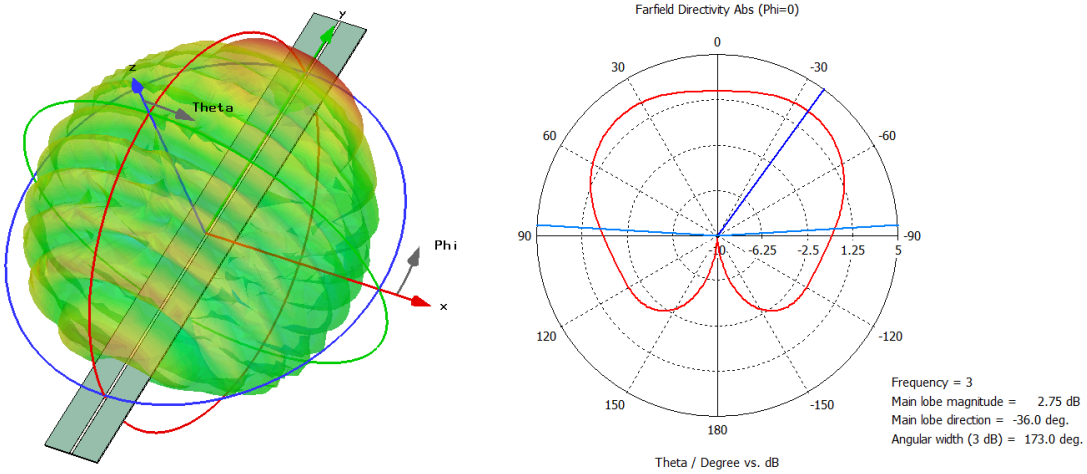

Figure 4.3: Far field radiation from a microstrip line

4.2 Strip Lines

Strip lines can be seen as the logical root of the microstrip lines, which can be seen as well as a several developments for the traditional coaxial lines as shown in figure 4.4.

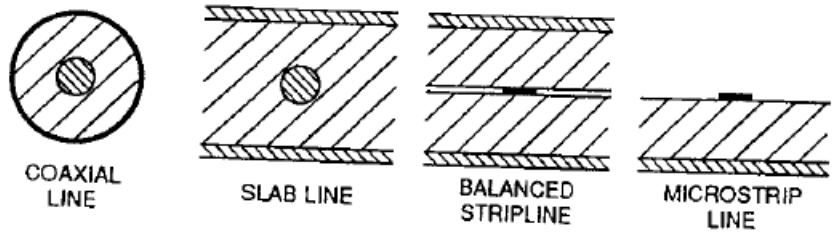

Figure 4.4: Development of the coaxial cable to the strip and microstrip lines [25]

In addition to having two conductors, the strip line has the advantage of having a homogenous dielectric medium instead of the air-dielectric compensation seen in the microstrip lines. This leads to the line being able to hold TEM waves instead of the quasi TEM in the microstrip line [24]. The strip line has more symmetrical fields' distributions as well, as shown in figure 4.5.

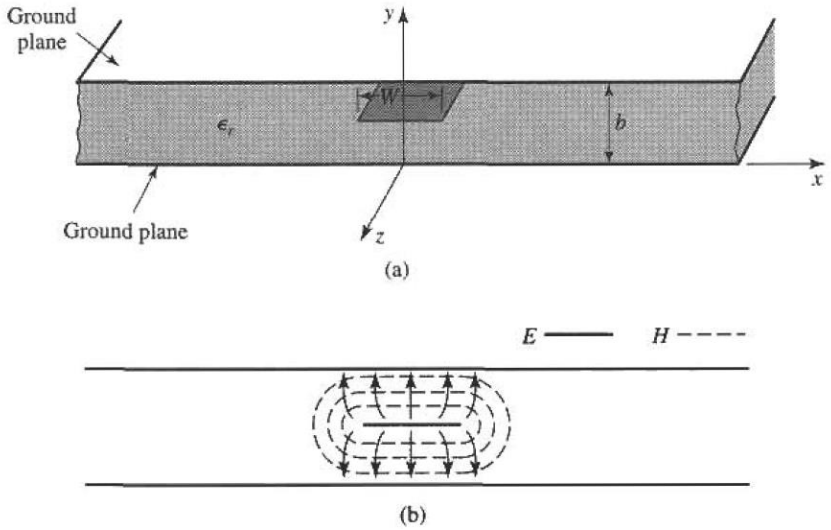

Figure 4.5: Strip line geometry and field distributions [24]

The wavelength of propagation inside a strip line is given by [24]:

$$\lambda_g = \frac{\lambda_0}{\sqrt{\varepsilon_r}} \tag{4.1}$$

Equations to determine the characteristic impedance and to synthesize the width for a given impedance might be found at the references [24] [21]. The strip line might be integrated with a microstrip antennas via various feeding methods. Since it is of our interest to shield the antenna pattern we will compare the strip line with the microstrip line in terms of the far field radiation. A strip line of the same ground and substrate's planar dimensions with an impedance of 50 ohm is examined at the same test frequency of last section. Figure 4.6 shows the animated distribution of the E-field magnitude in the propagation plane for a constant time.

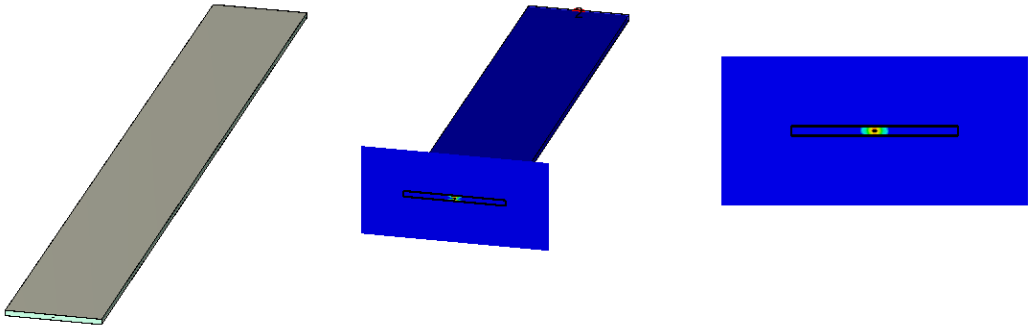

Figure 4.6: E-field magnitude distribution in the plane of propagation

From the figure we can see that the field is trapped inside the upper and lower metals and therefore we expect lower radiation especially in the vertical direction. Figure 4.7 shows a 3-D far field pattern along the 2-D far field pattern of the directivity in the propagation plane (ϕ=0) confirming our expectations.

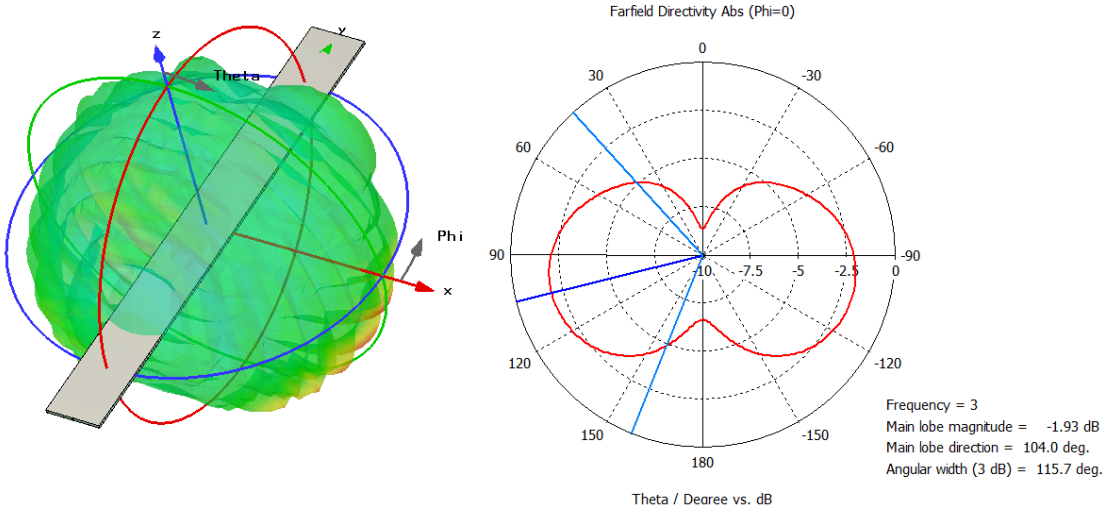

Figure 4.7: Far field radiation from a strip line

Figure 4.8 shows a comparison between strip line and microstrip line, the main lobe magnitude of strip line is 4.68 dB lower than the main lobe of a microstrip line. In addition the maximum direction of radiation is in the horizontal plane (due to the opening in the sides), which is usually not the direction of the main lobe for most microstrip antennas. For these reasons the use of strip lines is preferable over microstrip lines to shield the pattern and reduce the radiation loss in the microwave printed circuits.

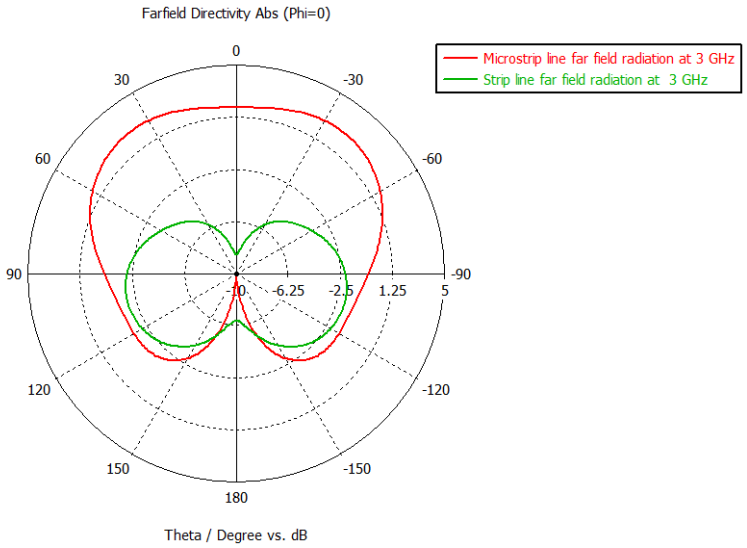

Figure 4.8: Far field radiation from a microstrip line versus a strip line

4.3 The Proposed Shielded Line Aantenna Structure

It is obvious for us now that the use of strip line is superior over microstrip lines to reduce the spurious radiation. The idea in the shielding method is to implement all the feed network and the microwave devices in the circuit using strip line technology, and wherever a deployment of antenna is required an aperture in the upper ground is formed and a microstrip antenna is placed there, the feed to the antenna is electromagnetic (i.e. proximity coupling). Figure 4.9 shows a frontal and vertical views demonstrating the proposed structure.

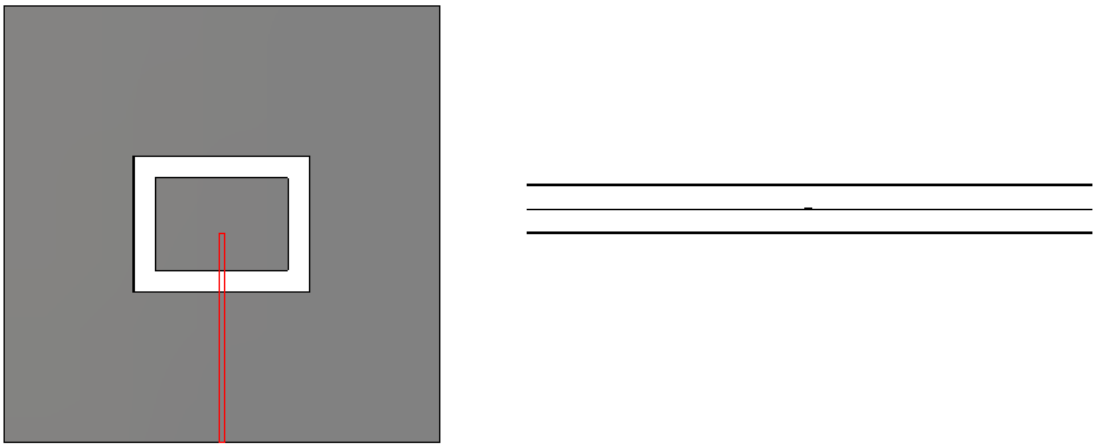

Figure 4.9: Frontal and vertical views for the proposed shielded antenna structure

Despite this structure being not that useful for a single element with a direct singular feed line, for more complicated structures such as the monopulse antenna, the shielding will be more important. The design of the antenna follows the simple rectangular microstrip patch analysis mentioned in chapter 3, however for matching and good radiation characteristics the dimensions of the line insertion under the patch and the aperture dimensions are optimized.

4.4 Conventional versus Shielded Single Microstrip Antenna

A brief evaluation of the proposed single element structure is provided here with the conventional microstrip antenna as a reference. Both designs are done using FR-4 substrates and at a frequency of 3 GHz for the sake of comparison. The design of the conventional microstrip antenna is done using the steps mentioned in section 3.3 and 3.4 with the inset line matching technique. Table 4.1 shows the antennas geometrical parameters, figure 4.10 shows the constructed antenna.

Table 4.1: The conventional single patch antenna geometrical parameters

Parameter symbol	**Description**	**Value (mm)**
h	Substrate height	1.6
t	Metal thickness	0.1
W	Patch width	30.429
L	Patch length	22.9
W_{50}	Width of the 50 ohm microstrip line	2.868
y	Insertion length for the inset line	9.55
W_c	Width of the inset line gap	0.8

Figure 4.11 shows the return loss of the antenna, the matching led to -16.45 dB return loss at the resonant frequency, and 2 VSWR bandwidth of about 45 MHz. The antenna radiation pattern is shown in figure 4.12; the antenna achieved maximum directivity of 7.7 dBi and a side lobe level of -16.3 dB.

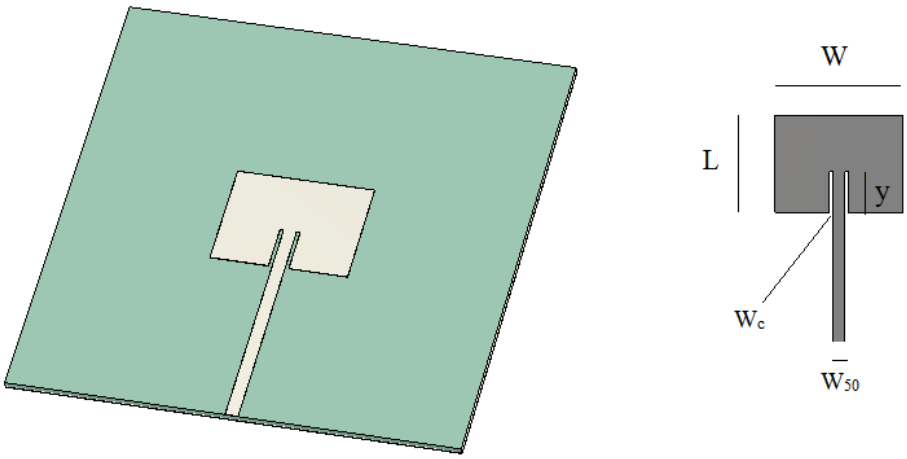

Figure 4.10: Single microstrip antenna geometry and parameters

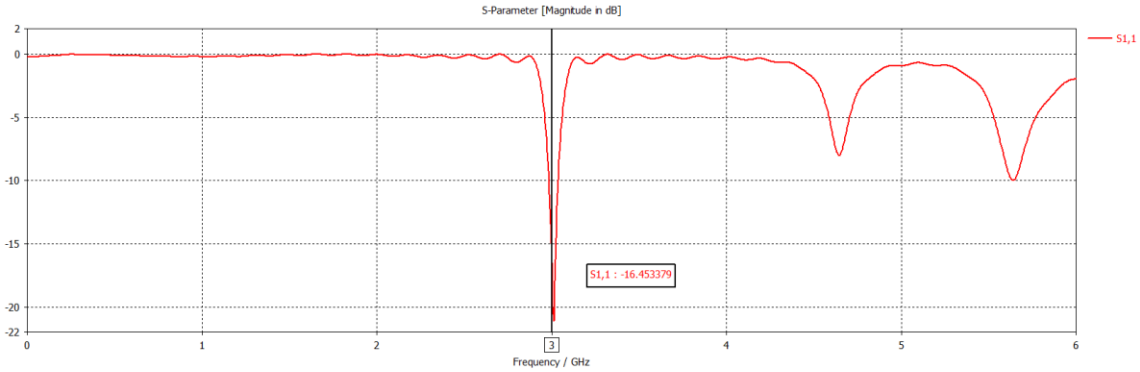

Figure 4.11: Return loss of the conventional patch

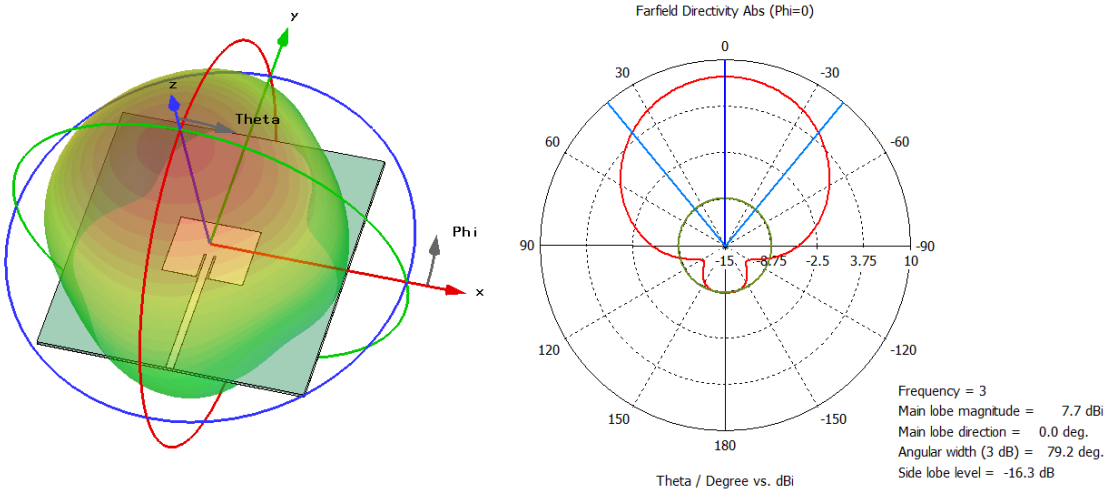

Figure 4.12: Radiation pattern for the single microstrip

The proposed antenna is designed first by the conventional way for proximity rectangular patch and then it is optimized using CST software for the best possible radiation and matching conditions. Table 4.2 shows the geometrical parameters of the proposed antenna. Figure 4.13 shows the additional antenna geometrical parameters on the conventional design.

Table 4.2: The proposed single patch antenna geometrical parameters

Parameter symbol	**Description**	**Value (mm)**
h	Half of the substrate height	3.3
t	Metal thickness	0.1
W	Patch width	30.429
L	Patch length	21.2
W_{50}	Width of the 50 ohm strip line	1.235
N	Line insertion under the patch	8.5
I_1 , I_2	Cut gap width	5

The return loss for the proposed antenna is shown in figure 4.14, the matching has led to –18.79 dB return loss at the resonant frequency, and a -10 dB bandwidth of about 106 MHz, the antenna radiation pattern with a maximum directivity of 7.47 dBi and a side lobe level of -12.8 dB is shown in figure 4.15.

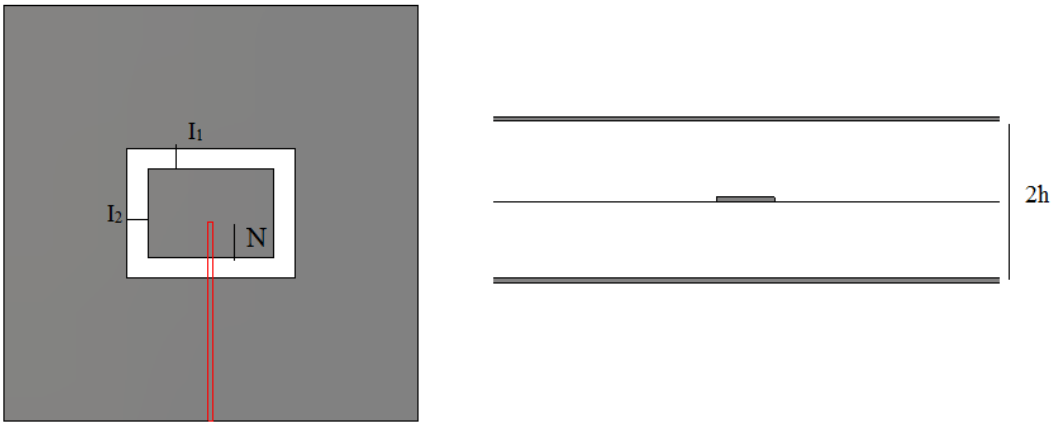

Figure 4.13: Additional geometrical parameters for the proposed antenna

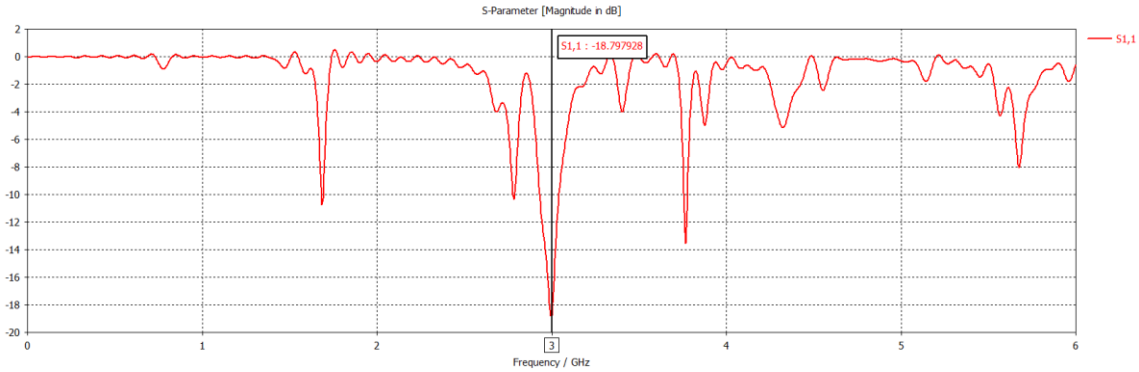

Figure 4.14: Return loss for the proposed antenna

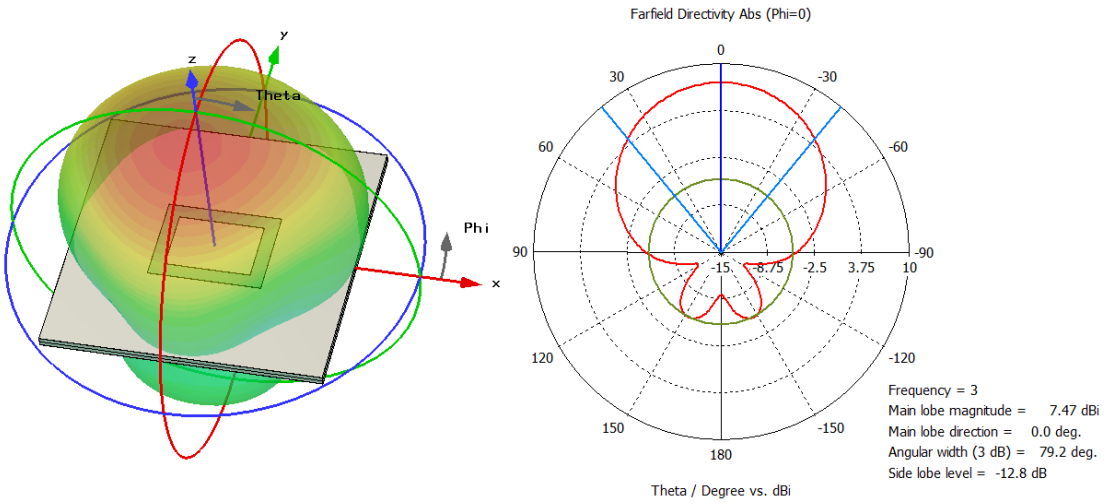

Figure 4.15: Radiation pattern for the proposed antenna

Table 4.3 shows a summary comparison between the two antennas, in terms of bandwidth the proposed antenna has broader bandwidth due to the proximity coupling, however such property for the shielding method in general depends on the type of the feeding network and the devices in the circuit; circuits containing narrow band elements will have a narrow band overall response. The proposed structure has higher side lobe level than the conventional method due to the fact that the main beam is very wide and the spurious radiation of the microstrip will add up in the direction of the main lobe instead of creating minor lobe. However, a closer look to the spurious radiation of strip line (figure 4.7) shows that the radiation is toward the metal opening in the sides, which is in the single element case more apparent since the main lobe is a wide vertical one. For arrays and networks with complicated integrated circuits, this will not be the case. Narrow patterns and patterns in beam forming network will be highly damaged by such spurious radiation as we will see in the next section.

Table 4.3: Performance comparison between single conventional patch antenna and the proposed antenna

	Conventional antenna	**Proposed antenna**
Resonant return loss (dB)	-16.45	-18.79
Bandwidth (MHz)	45	106
Maximum directivity (dBi)	7.7	7.47
Side lobe level (dB)	-16.3	-12.8

4.5 (2 by 2) Shielded Array versus Conventional Array

To prove the efficiency of the proposed technique an antenna with a feed network in between must be examined rather than the single element which already gave us an insight about the concept. A simple example to achieve that is the 2 by 2 planar microstrip array with a corporate feed as shown in figure 4.16, the λ/4 transformation feed is used [23], the single microstrip patch discussed in section 4.4 is used as an element here.

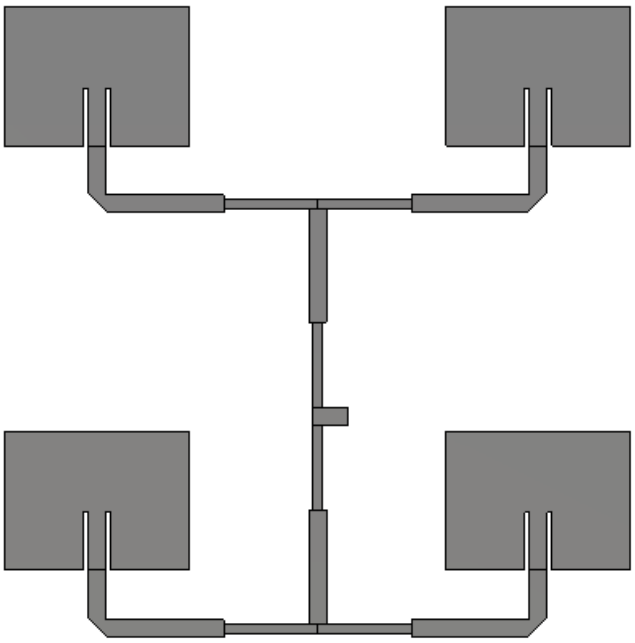

Figure 4.16: 2 by 2 planar microstrip array with corporate feed

Figure 4.17 shows the radiation characteristics of the normal array structure, where a maximum directivity of 12.3 dBi has been realized with a side lobe level of -14.8dB.

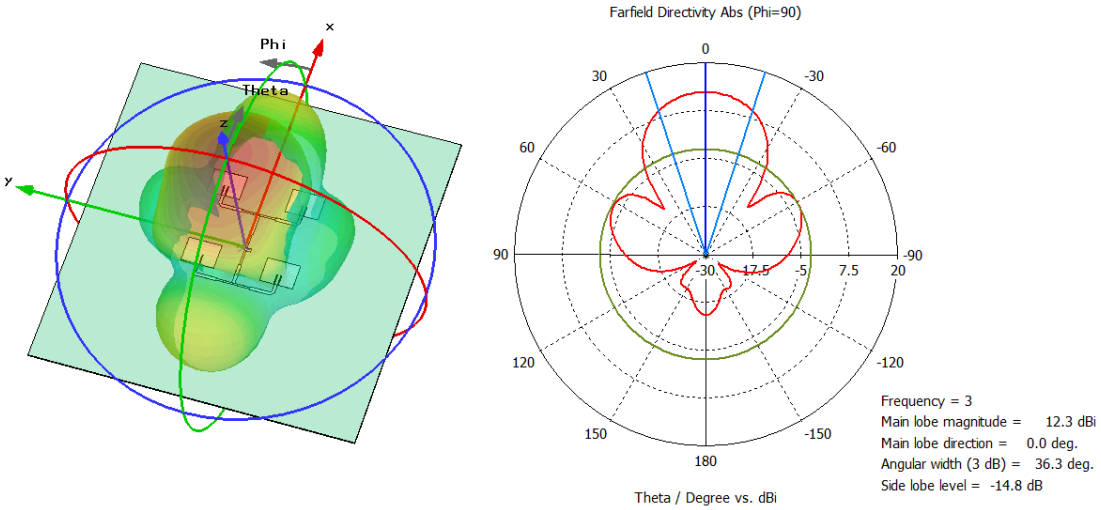

Figure 4.17: Radiation pattern for the 2 by 2 conventional array

The shielded version of this antenna is shown in figure 4.18. The feed network is designed based on the same principle of quarter wavelength transformer but it is implemented through strip lines. The single element in section 4.4 is used to form the array.

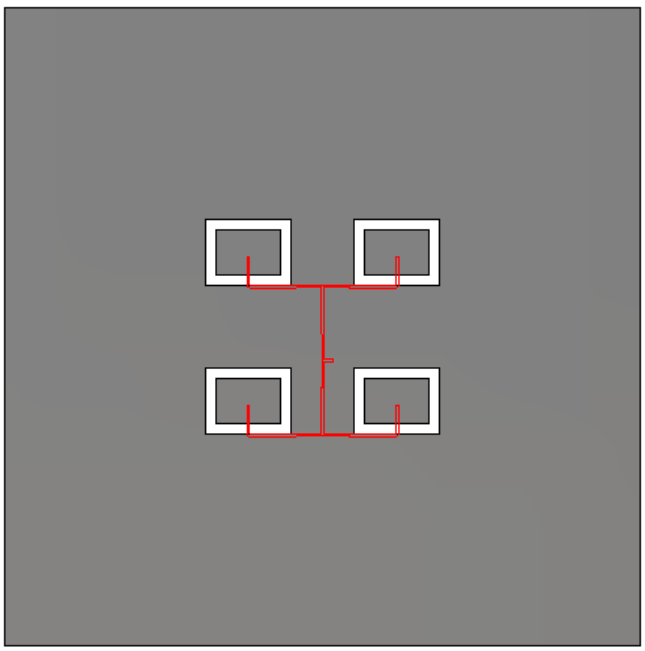

Figure 4.18: The proposed shielding technique on 2 by 2 microstrip array

The radiation characteristics of the shielded array structure has maximum directivity of 12.8 dBi with an improved side lobe level of -16.5dB, this is shown in figure 4.19.

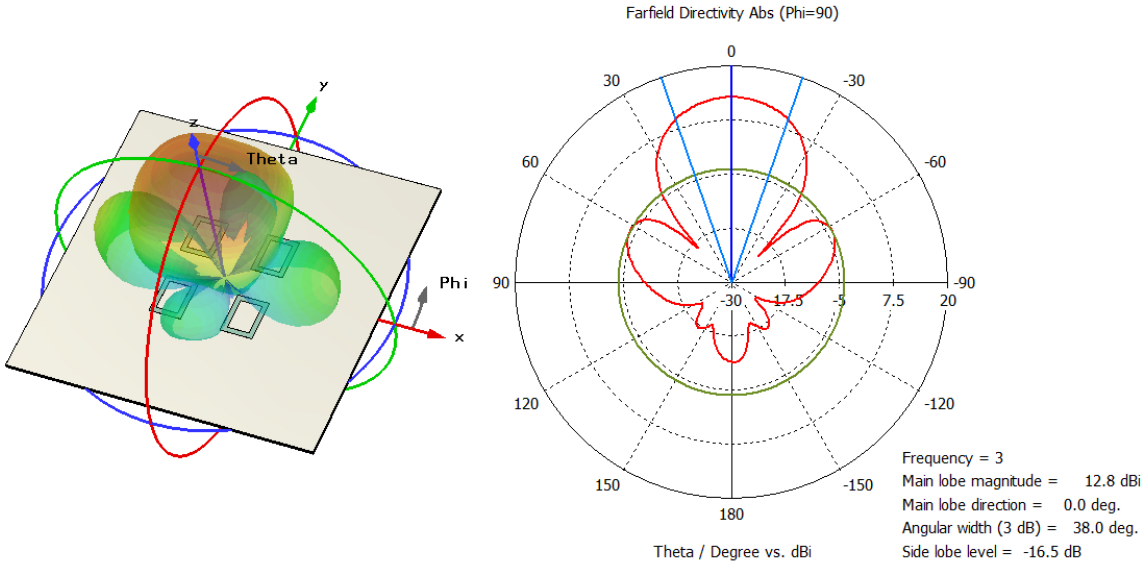

Figure 4.19: Radiation pattern for 2 by 2 shielded array

Figure 4.20 shows the radiation patterns for both arrays for comparison. The shielded array has deeper nulls which is closer to the ideal planar array pattern (which has minus infinite null in dB. The suppression of the microstrip lines spurious radiation dropped the sidelobes further as well. Greater impact is expected for larger arrays.

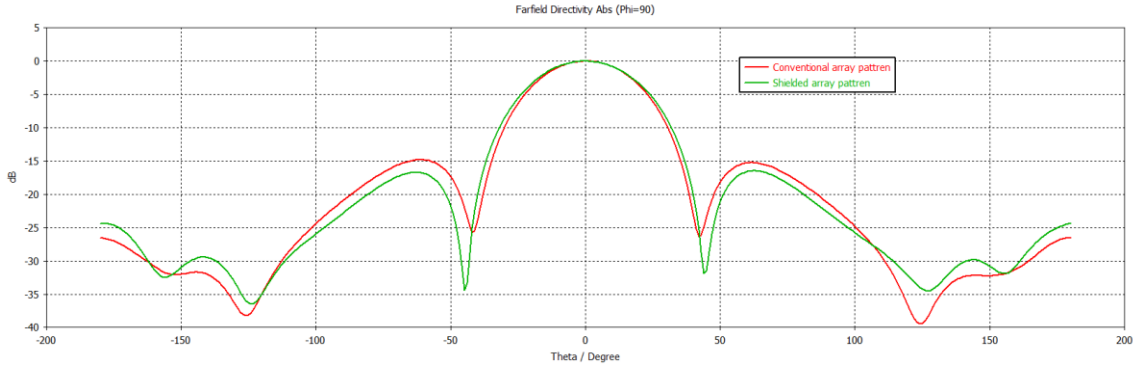

Figure 4.20: Radiation pattern for conventional versus shielded 2 by 2 microstrip array

Chapter 5

MICROSTRIP MONOPULSE ANTENNA

5.1 90^0 Hybrid Couplers

The 90^0 hybrid is the building block for our comparator as discussed in section 2.3.The general structure and design steps are mentioned in section 3.5. The system characteristic impedance is the standard 50 ohm and therefore, according to equations 3.11 and 3.12, Z_{series} and Z_{shunt} for the hybrid coupler will be 35.35 and 50 ohm respectively. Figure 5.1 shows the geometries of the designed hybrid coupler. The same substrate as in the previous chapter is used at the same frequency (FR-4 at 3GHz). Table 5.1 shows the list of the parameters. Note that due to the difference in the effective permittivity for each line they will not have the same estimated propagation wavelength (equation 3.6).

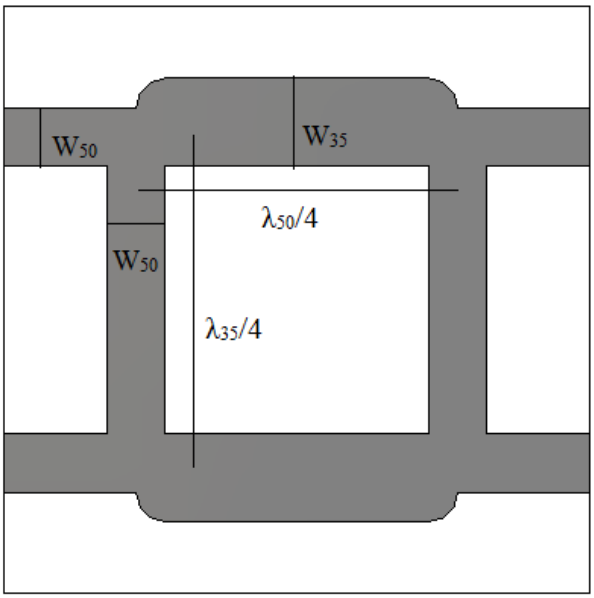

Figure 5.1: Microstrip Hybrid coupler geometries

Table 5.1: The microstrip hybrid coupler geometrical parameters

Parameter symbol	Description	Value (mm)
h	Substrate height	1.6
t	Metal thickness	0.1
W_{50}	50 ohm line width	2.981
W_{35}	35 ohm line width	4.479
λ_{50}	50 ohm line propagation wavelength	13.71
λ_{35}	35 ohm line propagation wavelength	13.48

At the operating frequency the scattering matrix should be as close as possible to the ideal coupler matrix (equation 3.10). For instant if port one is the input port, port 1 and 4 are isolated (i.e. ideally S_{14} is infinitely negative), and the coupling between 1 to 2 and 1 to 3 will be equal (i.e. S_{12}, S_{13} both have a magnitude of -3dB) with 90^0 shift. Since the device is symmetric the rest of the matrix is satisfied accordingly. Figure 5.2 shows the magnitude of the first raw of the S parameters, where the desired properties are satisfied at the operating frequency ($S_{12} = S_{13} = -3.3$dB).

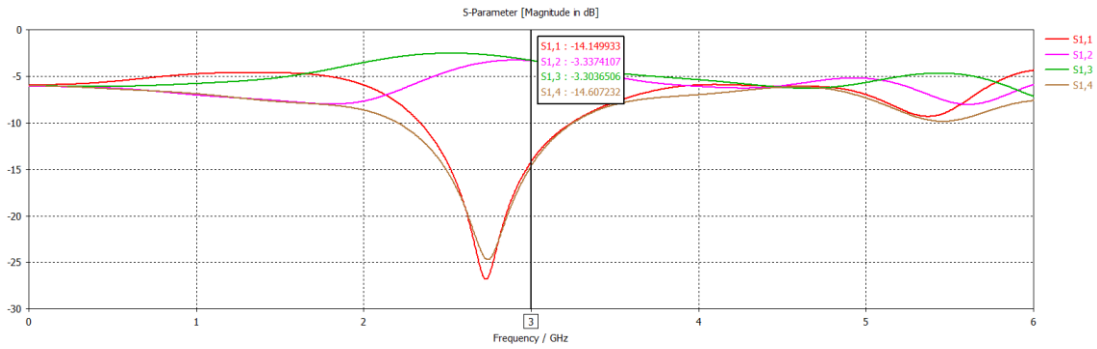

Figure 5.2: Magnitude of the first raw of the scattering matrix at the operating frequency

Figure 5.3 shows the phase shift between S_{12} and $S_{13,}$ a phase shift of 91.55^0 is recorded.

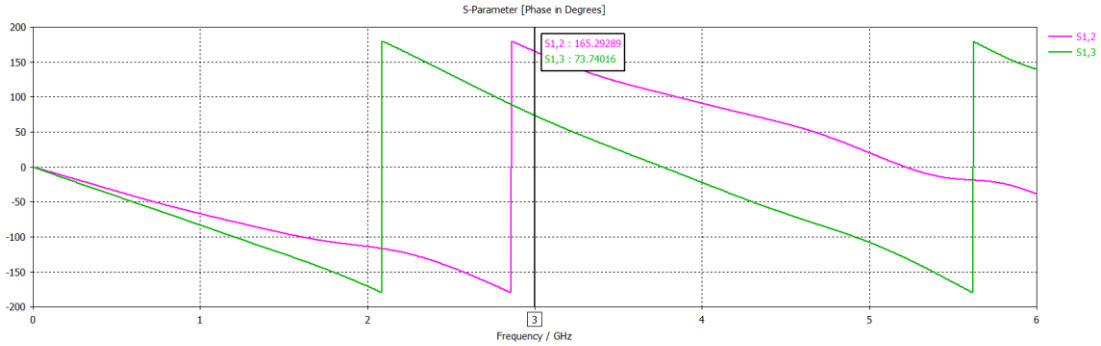

Figure 5.3: Phase shift between S_{12} and S_{13} at the operating frequency

The same design might be realized using strip lines. Figure 5.4 show a strip line hybrid coupler structure, with Table 5.2 showing the geometrical parameters. Note here that the wavelength of propagation is the same for all lines on the same substrate and frequency as given by equation 4.1.

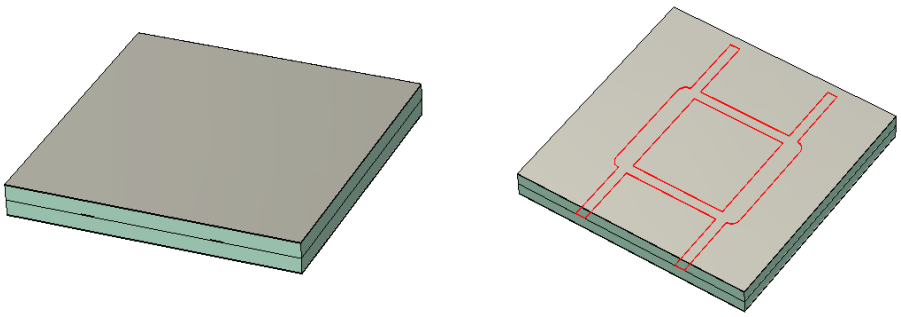

Figure 5.4: Strip line 90^0 hybrid coupler

Table 5.2: The strip line hybrid coupler geometrical parameters

Parameter symbol	Description	Value (mm)
h	Half of the Substrate height	3.3
t	Metal thickness	0.1
W_{50}	50 ohm line width	1.235
W_{35}	35 ohm line width	2.285
λ_{50}	50 ohm line propagation wavelength	11.918
λ_{35}	35 ohm line propagation wavelength	11.918

Figure 5.5 shows the corresponding magnitude of the first raw of the S parameters and figure 5.6 shows the phase shift between S_{12} S_{13}.

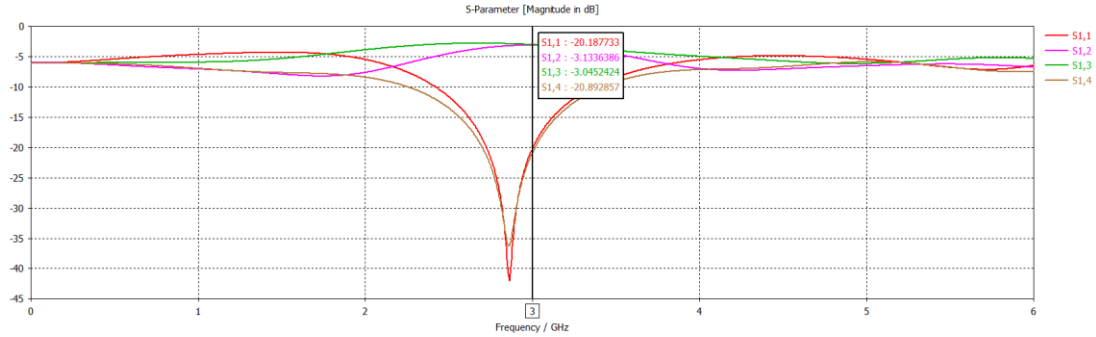

Figure 5.5: Magnitude of the first raw of the scattering matrix at the operational frequency for the strip line hybrid

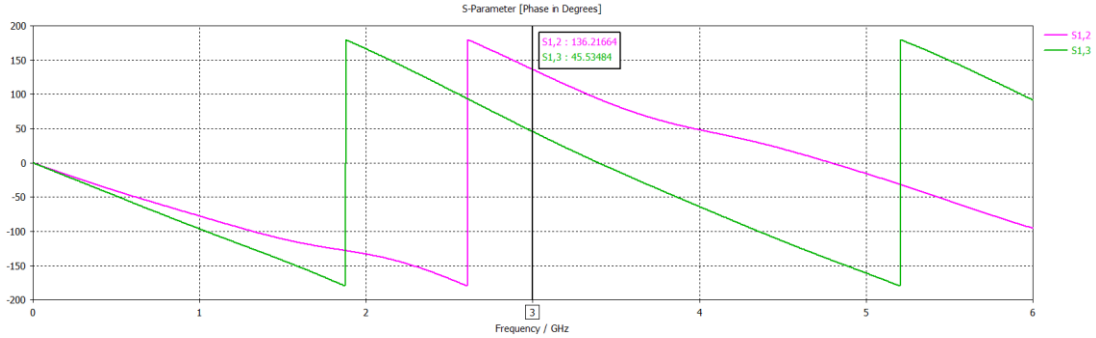

Figure 5.6: Phase shift between S_{12} and S_{13} at the operating frequency for the strip line hybrid

From the graphs we can see that S_{12} =-3.13dB, S_{13} = -3.04dB and the phase shift between them is 90.68^0, which meets our design aims.

5.2 Microstrip Microwave Comparator

A microwave comparator is used to generate the sum and difference patterns in the monpulse system, ideally for A, B, C and D patterns, the following patterns are generated:

$$\sum = A + B + C + D \tag{5.1}$$

$$\Delta_1 = (A + C) - (B + D) \tag{5.2}$$

$$\Delta_2 = (C + D) - (A + B) \tag{5.3}$$

Such a device can be realized by different methods such as the use of quadrature hybrids discussed in previous section. The block diagram of such a realization is shown in figure 2.7. However due to the nature of the power division in such a method, the generated signals will be multiplied by a factor of one half. In addition a forth signal representing the diagonal difference is generated through the operation and it is not used. Figure 5.7 shows the use of quadrature hybrid couplers to form a comparator, keeping into consideration that the phase shifts in figure 2.7 must be achieved either by the source signals or by additional line lengths as we will apply later.

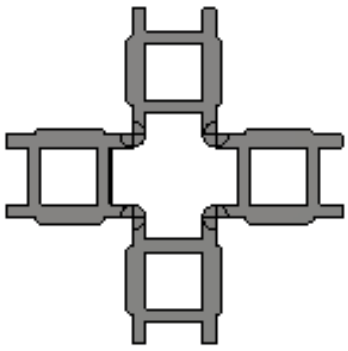

Figure 5.7: Microstrip comparator using 90^0 hybrids

The edges are connected through a smooth circular arcs rather than a 90^0 edge to reduce the reflection and the spurious radiation.

To test the structure four simple step sine waves with the same amplitude were used, the same frequency (3GHz) and the proper phase shift as listed in table 5.3. The input signals are shown in figure 5.8.

Table 5.3: Phase and time shifts for the test sine wave signals

Port	Phase shift (degree)	Time shift (ns)
1	180	0.16666
2	90	0.08333
3	90	0.08333
4	0	0

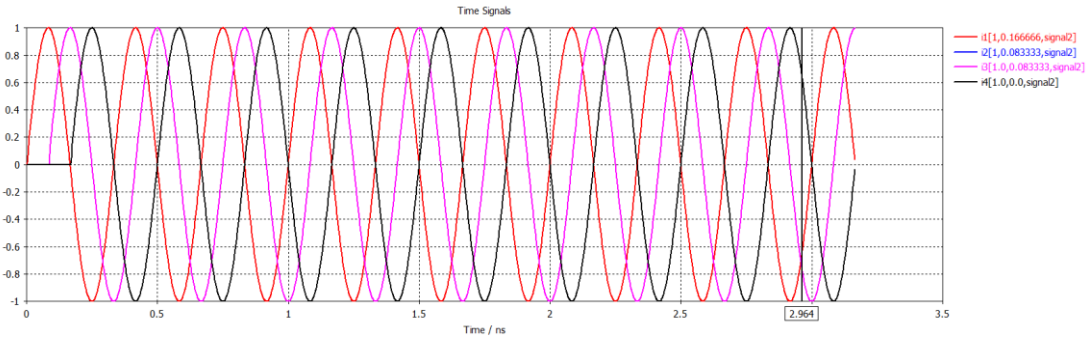

Figure 5.8: Test sine waves signals

The expectation is to have only a sum signal which is a sinewave signal with amplitude of 2 (i.e. [sin (wt) +sin (wt) +sin (wt) +sin (wt) =4sin (wt)] but then divided by 2). Figure 5.9 shows the output signals. It meets our expectation in the steady state. Now finally the same structure can be constructed by strip lines.

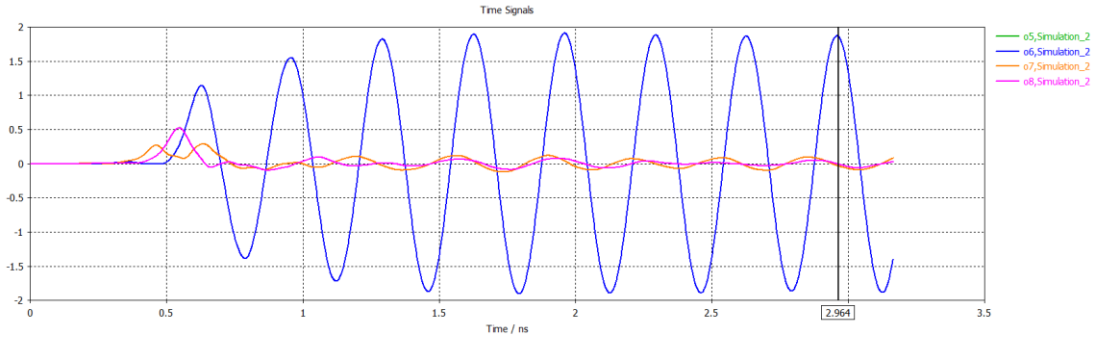

Figure 5.9: comparator output for the test signals

5.3 Microstrip Monopulse Antenna

Combining the realization for the radiator and the comparators the system can be finally constructed. We will use the 2 by 2 antenna array designed in section 4.5 (shown in figure 4.16) to generate the beams, the comparator will be printed in the middle for compactness. The delays can be realized by additional lengths, each λ is corresponding to a 360^0 phase shift. Figure 5.10 shows the structure of the design.

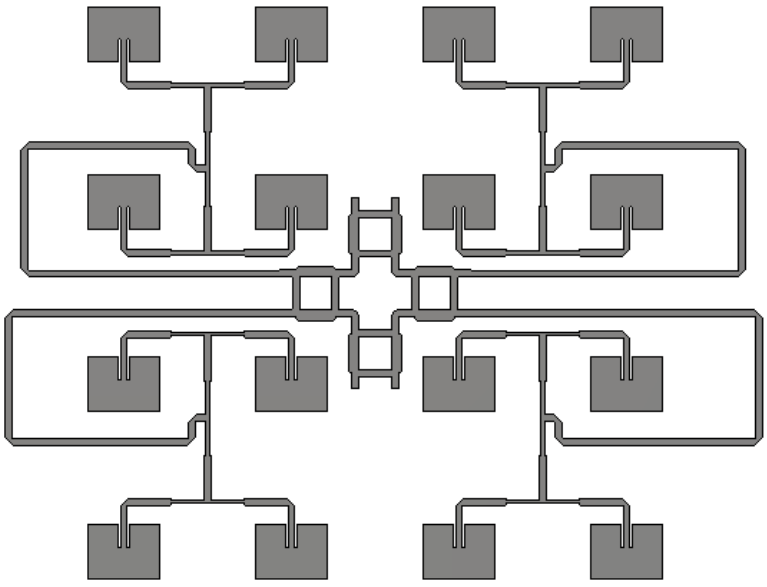
Figure 5.10: Microstrip monopulse antenna structure

The following figures (5.11 – 5.17) show the generated radiation patterns for the sum and difference patterns in both ϕ=0 and ϕ=90 planes.

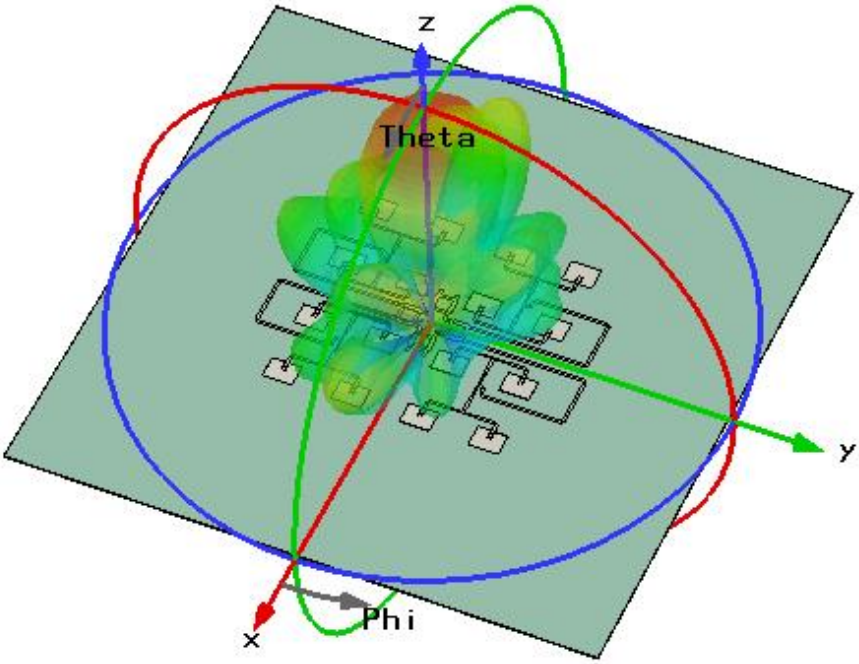

Figure 5.11: 3-D sum pattern

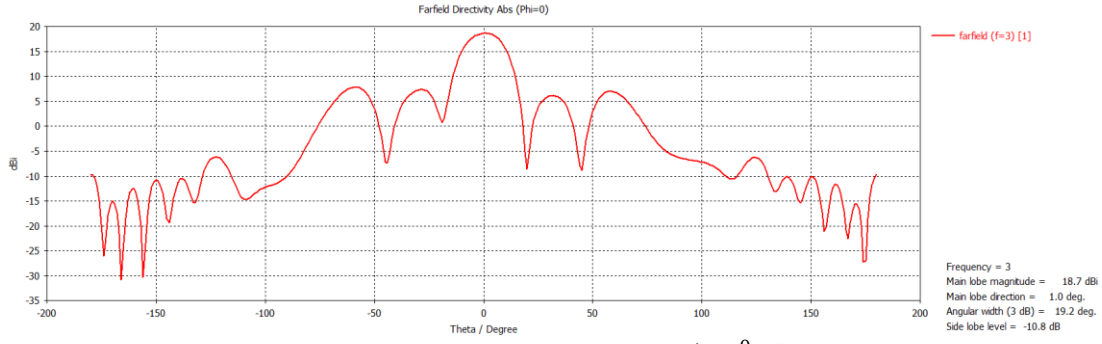

Figure 5.12: 2-D sum pattern in $\phi=0^0$ plane

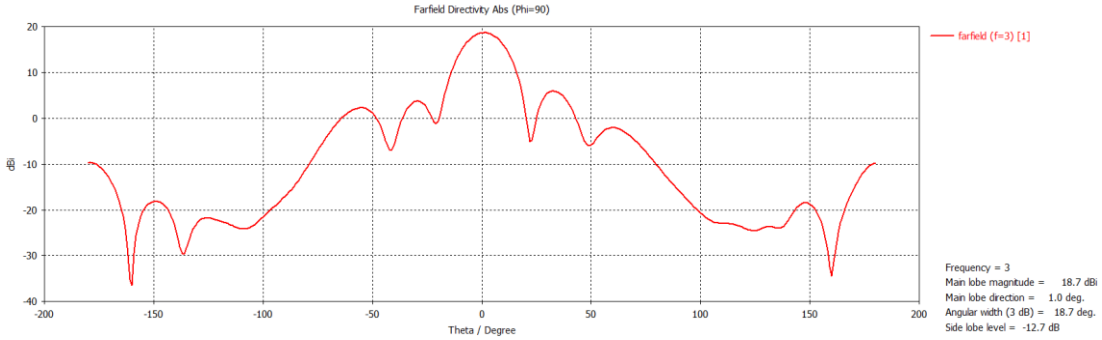

Figure 5.13: 2-D sum pattern in $\phi=90^0$ plane

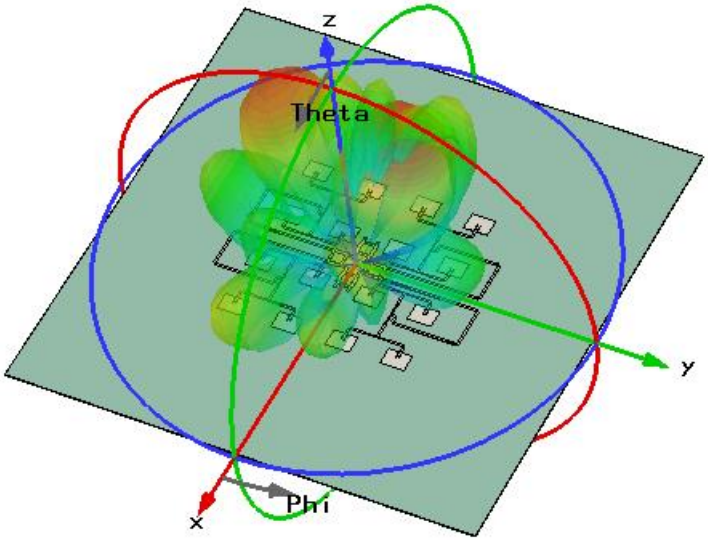

Figure 5.14: 3-D difference pattern ($\phi=90^0$)

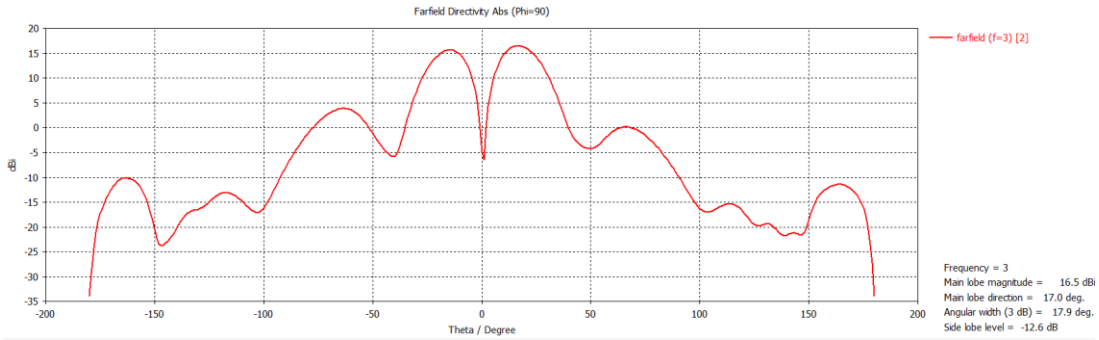

Figure 5.15: 2-D difference pattern in $\phi=90^0$ plane

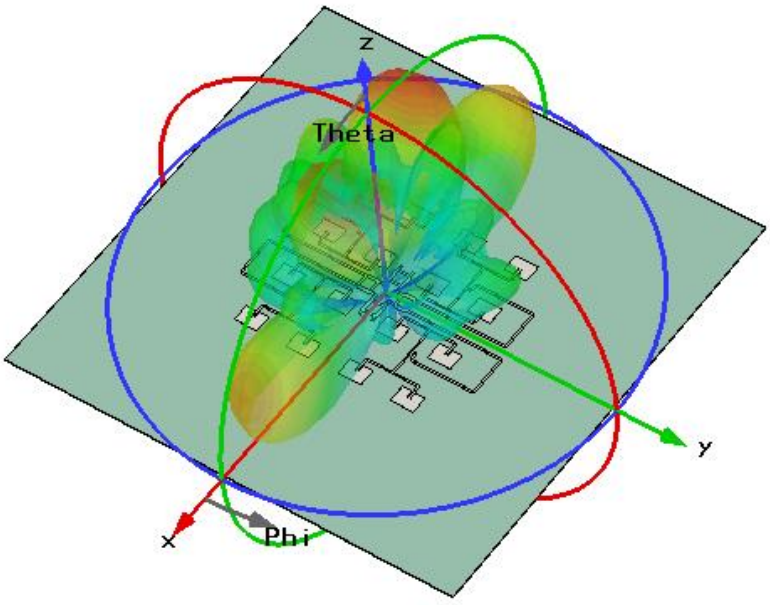

Figure 5.16: 3-D difference pattern ($\phi=0^0$)

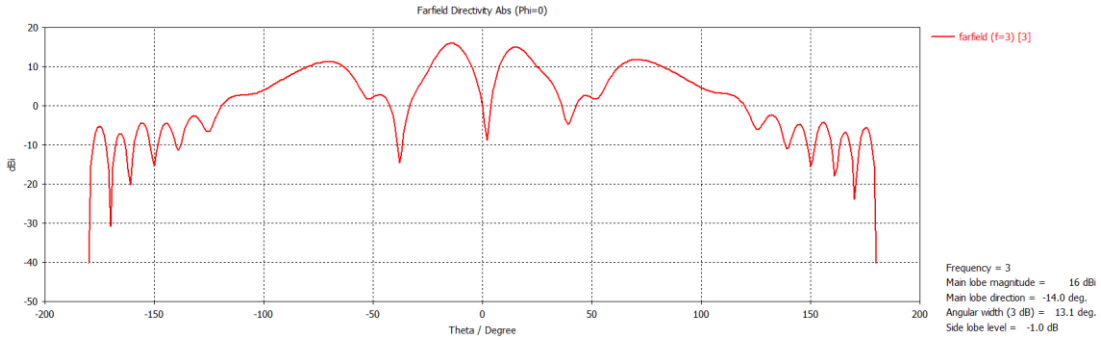

Figure 5.17: 2-D difference pattern in $\phi=0^0$ plane

The monopulse antenna exhibited a sum maximum directivity of 18.6 dBi, with sidelobe levels of -10.8dB in the $\phi=0^0$ plane and -12.7dB in the $\phi=90^0$ plane. In term of the difference characteristics at the plane $\phi=90^0$ the null depth is -22.9dB shifted by 1^0, -24.7dB null depth is reported in the plane $\phi=0^0$ with a null shift of 2^0.

5.4 Shielded Microstrip Monopulse Antenna

In this section the method proposed in section 4.3 will be examined and its efficiency to improve the monopulse antenna performance will be evaluated. Figure 5.18 shows the structure of the shielded device.

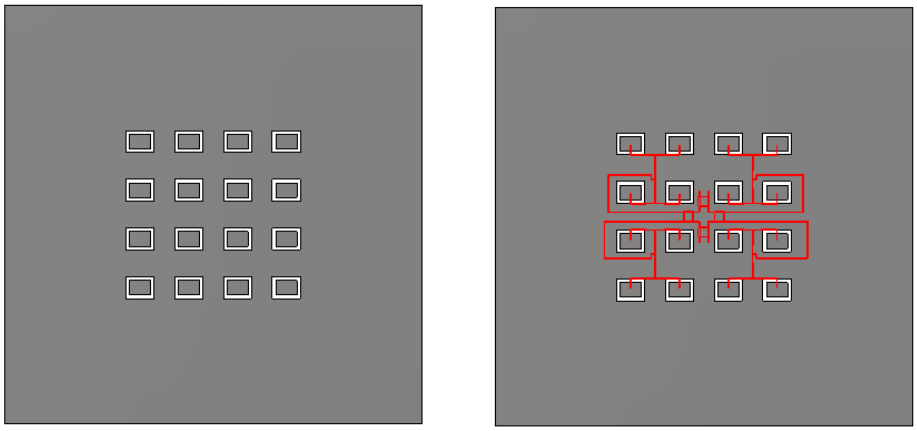

Figure 5.18: Shielded monopulse antenna structure

Figures 5.19-21 show the three dimensional patterns for the shielded antenna.

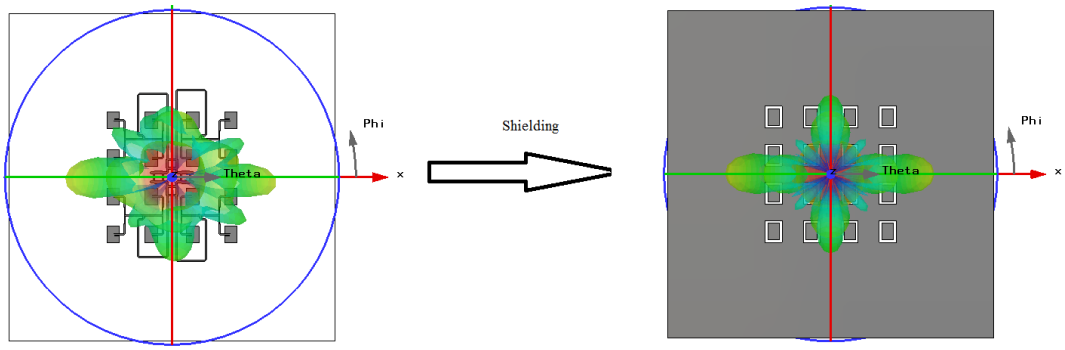

Figure 5.19: 3-D sum pattern for shielded antenna

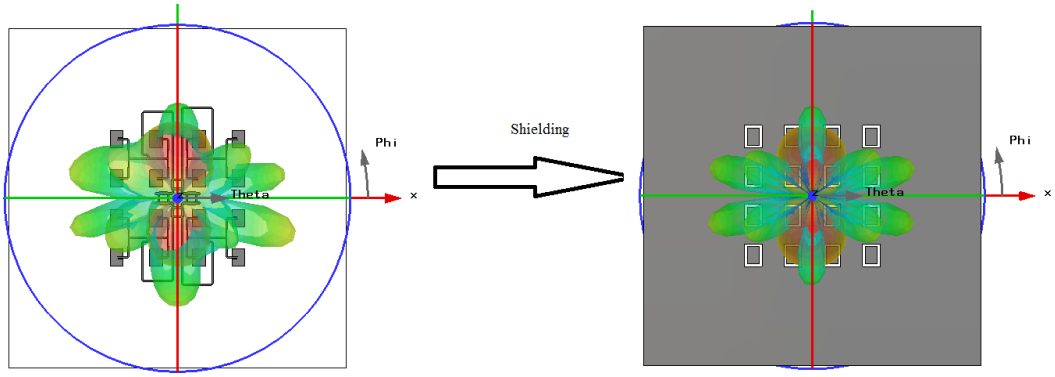

Figure 5.20: 3-D difference pattern ($\phi=90^0$) for shielded structure

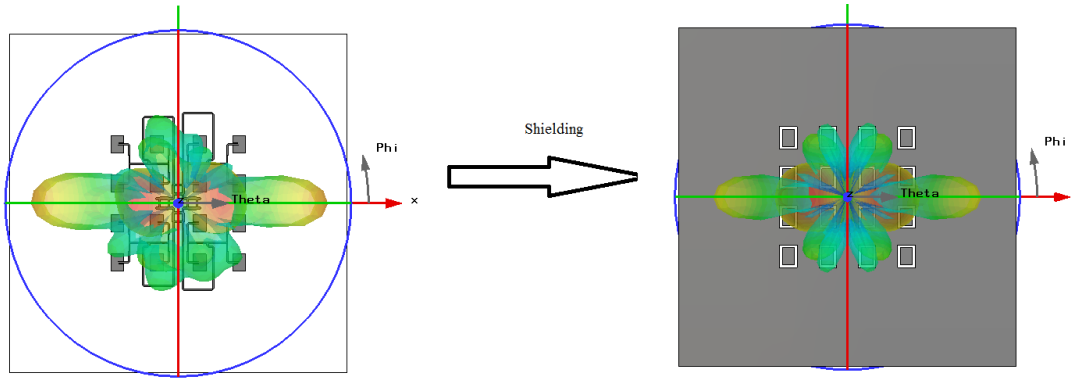

Figure 5.21: 3-D difference pattern ($\phi=0^0$) for the shielded structure

Comparing the previous figures (5.19-21) with the ones in section 5.3, we can see that all minor lobes due to feed network spurious radiation are reduced considerably, the symmetry of the shape in addition to the deeper nulls assures that fact. Figures 5.22-25 compare the 2-D patterns of the shielded array with the one designed in section 5.3.

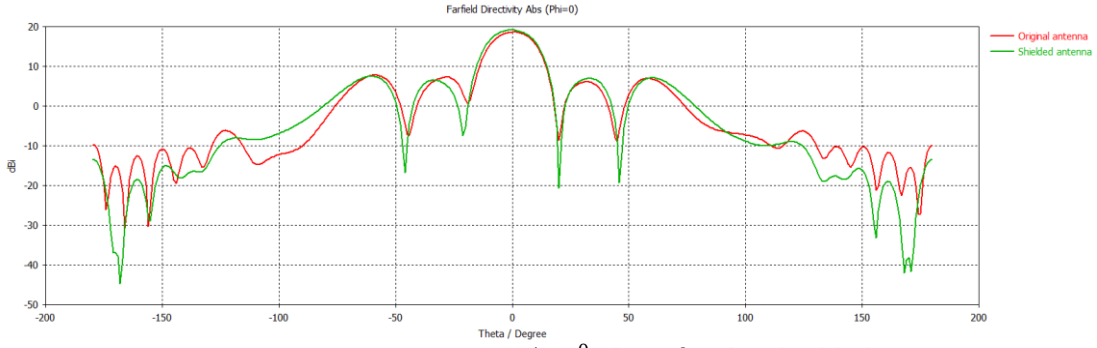

Figure 5.22: 2-D sum pattern in $\phi=0^0$ plane for the shielded antenna

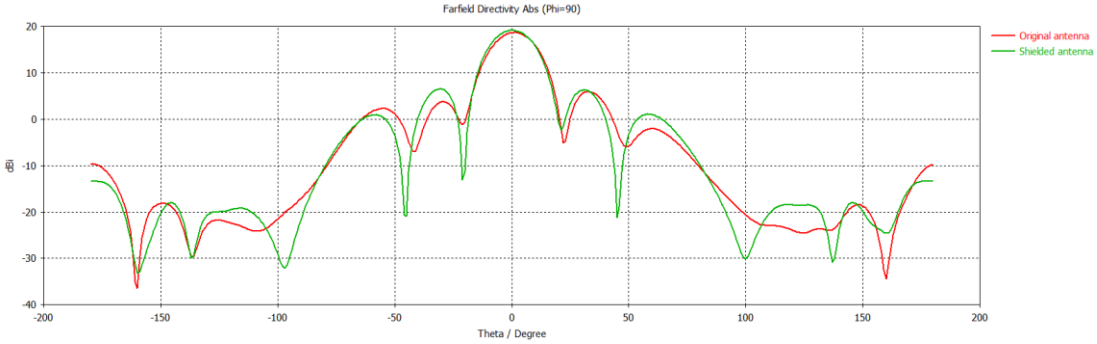

Figure 5.23: 2-D sum pattern in $\phi=90^0$ plane for the shielded antenna

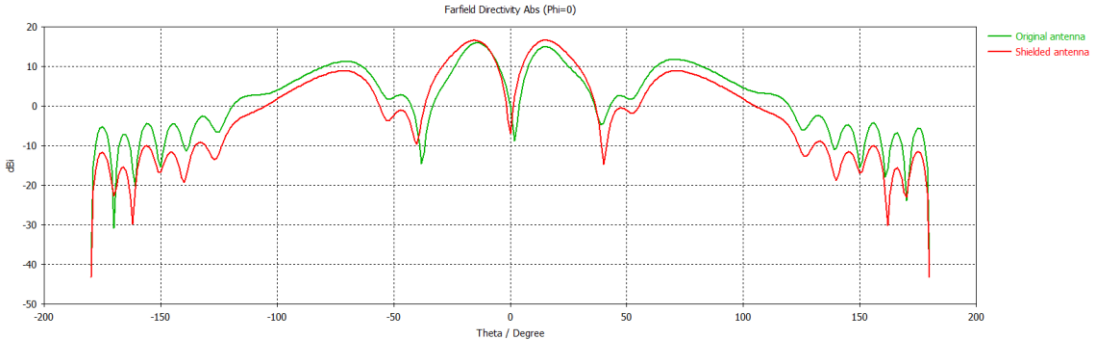

Figure 5.24: 2-D difference pattern in $\phi=0^0$ plane for the shielded antenna

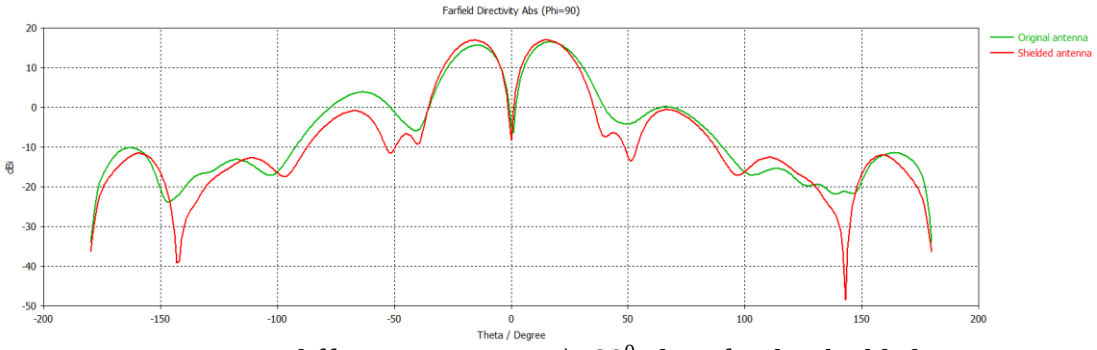

Figure 5.25: 2-D difference pattern in $\phi=90^0$ plane for the shielded antenna

The null depths of the shielded array are exactly at 0^0 due to the symmetry of the shielded shape; the nulls in the sum patterns are deeper indicating closer shape to the ideal pattern as discussed in section 2.4. After shielding the array a maximum directivity of 19.2 dBi was achieved, sum sidelobes are -12.6dB and -11.6dB in azimuth and elevation planes respectively, and null depths are -25.337dB and -23.626dB. The sidelobes of the difference patterns are reduced considerably as seen from figures 5.24 and 5.25. The symmetry in the shape will make it easier to develop algorithms to deal with the side noise. The only minor lobes remaining are due to the nature of the planer array, and they can be reduced by conventional sidelobe level (SLL) suppression techniques.

5.5 Further Improvement: Non-rectangular Planar Distribution

The sum pattern sidelobes hold significant importance in the monpulse performance since the sum pattern is used as transceiver and as a reference for the other patterns. Various methods have been used for sidelobe suppression for microstrip arrays [5], [29] and [30]. The change of distribution is one of the well-known methods. If we have a closer look at figure 5.18, we can see that each element individual pattern, in the sum case, is added to form the pattern shown in figure 5.19. However the contribution of each element sub-pattern to the main and the minor lobes varies according to the position. Elements near the center will be mostly contributing to the formation of the major lobe, while those in the sides will contribute less to that main lobe. On the other hand, side elements contribute more in the minor lobes. If we neglect the corner elements and adopt a non-rectangular elements distribution, we expect better sidelobes with some loss in the main lobe magnitude. Figure 5.26 shows the new distribution.

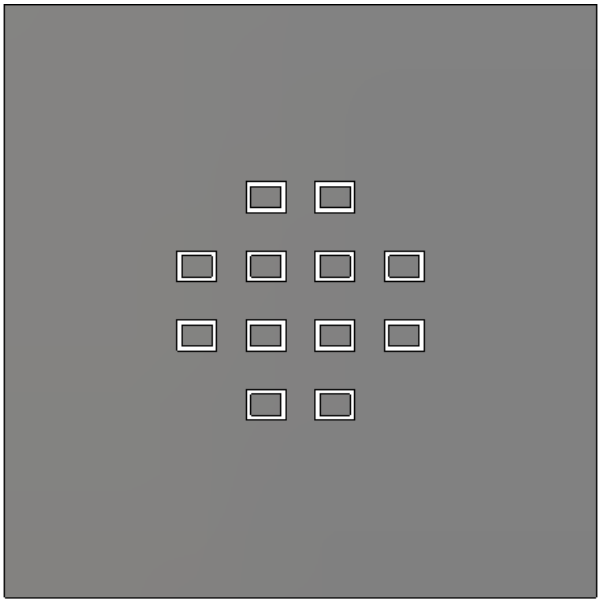

Figure 5.26: Non-rectangular monopulse antenna structure

Figure 5.27 shows the effect of the change of distribution on the sum pattern where the sidelobes are reduced.

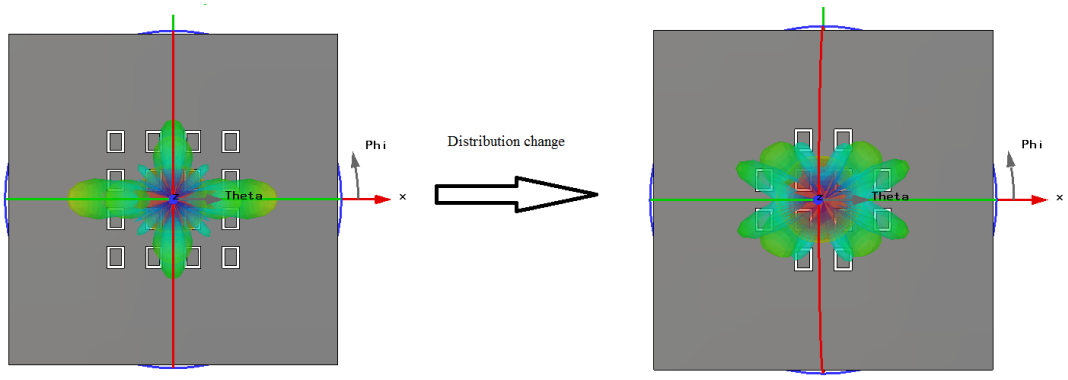

Figure 5.27: 3-D sum pattern for shielded antenna with the new non-rectangular elements distribution

Figures 5.28-31 compare the 2-D patterns of the non-rectangular distributed shielded array with the shielded array designed in section 5.4, and the conventional array designed in section 5.3.

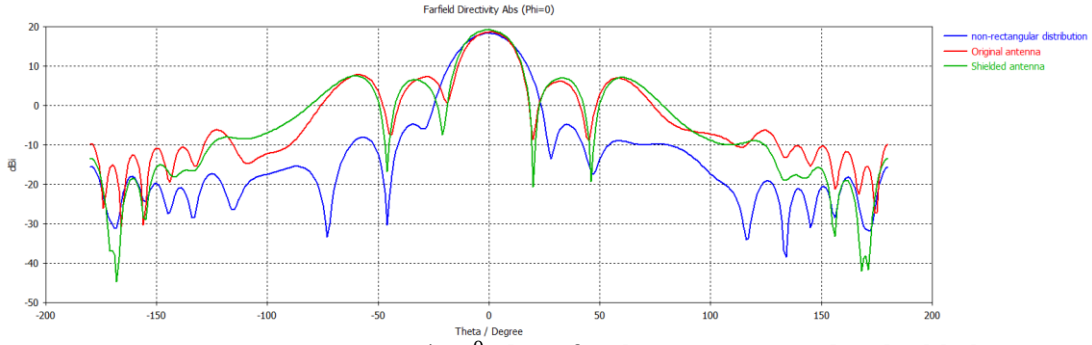

Figure 5.28: 2-D sum pattern in $\phi=0^0$ plane for the non-rectangular shielded antenna

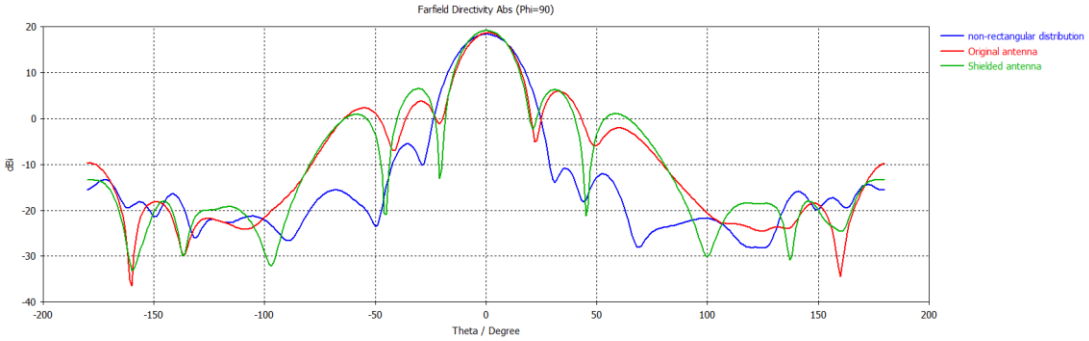

Figure 5.29: 2-D sum pattern in $\phi=90^0$ plane for the non-rectangular shielded antenna

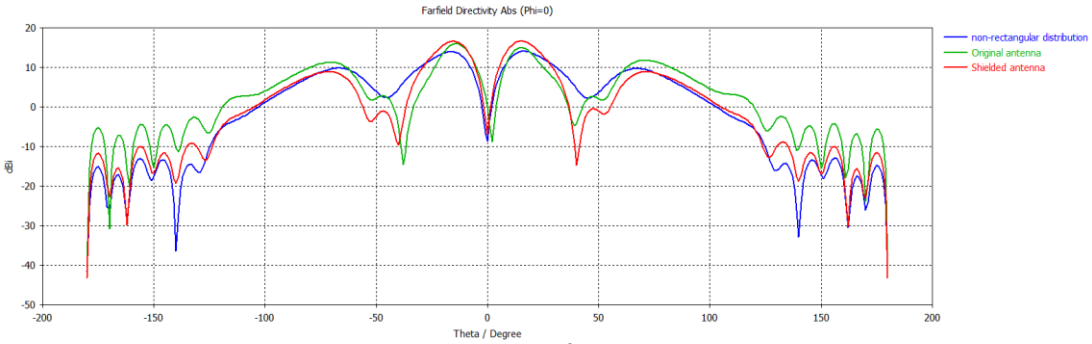

Figure 5.30: 2-D difference pattern in $\phi=0^0$ plane for the non-rectangular shielded antenna

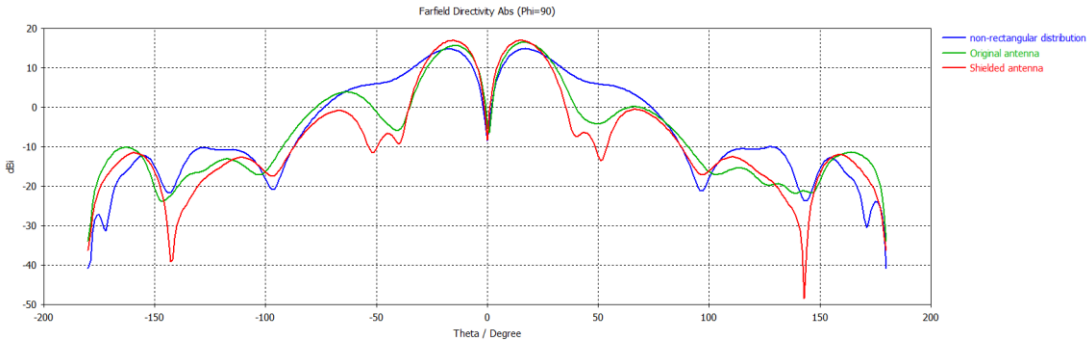

Figure 5.31: 2-D difference pattern in $\phi=90^0$ plane for the non-rectangular shielded antenna

The new non-rectangular shielded array sustained almost the same difference characteristics with nulls exactly at 0^0, and null depths of -23.367dB in the $\phi=90^0$ and -22.713dB in the $\phi=0^0$. In terms of the sum characteristics further improvements in the sidelobes were achieved with little sacrifice in the antenna maximum directivity. The

circular distributed shielded array achieved a maximum directivity of 18.4 dBi, sum sidelobes of -23.9dB and -23.1dB in azimuth and elevation planes respectively.

5.6 Summary of Results

In this work the conventional design of the monopulse microstrip antenna array has been improved through a novel method to shield the antenna pattern from the feed network spurious radiation, in addition a non-rectangular elements distribution has been adopted. The improved design has a symmetrical difference patterns with nulls exactly at zero. The sidelobes for the sum patterns has been dropped by about 10dB. Table 5.4 shows the summary of the results and the improvements achieved in terms of the radiation parameters.

Table 5.4: Summary of results

Parameter		**Conventional array**	**Shielded array**	**Non-rectangular shielded array**
Maximum Directivity (dBi)		18.6	19.2	18.4
Sum sidelobes (dB)	Elevation plane	-10.8	-11.6	-23.1
	Azimuth plane	-12.7	-12.6	-23.9
Null depth (dB)	Elevation plane	-24.73	-23.64	-22.71
	Azimuth plane	-22.9	-25.34	-22.713
Null position (degree)	Elevation plane	2	0	0
	Azimuth plane	1	0	0

Chapter 6

CONCLUSION

In this work a novel method to shield the radiation pattern of microstrip arrays from the feed network spurious radiation has been proposed. A 4 by 4 microstrip monopulse antenna array has been considered as a case study. The proposed method proved its efficiency for both microstrip arrays and for microstrip monopulse antenna system.

Through this shielding, the conventional design of the monopulse microstrip antenna array has been improved by inducing a symmetrical sum and difference patterns, with difference nulls exactly at zero, also this step reduced all minor lobes due to feed network radiation considerably. In addition, to suppress minor lobes due to the array nature a non-rectangular elements distribution has been adopted, overall the system sidelobes where dropped by 10dB.

REFERENCES

[1] Mark A. Richard, James A. Scheer & Willian A. Holm (editors). (2010). *Principles of Modern Radar*, Vol. I: Basic principles. SciTech.

[2] Samuel M. Sherman & David K. Barton. (2011). *Monopulse principles and Techniques*. Artech House.

[3] IEEE Standards Board. (1997). *IEEE Standard Radio Definition*. IEEE Xplore.

[4] Hao Wang, Da-Gang Fang & X. G. Chen. (2006). A Compact Single Layer Monopulse Microstrip Antenna Array. *IEEE TRANSACTIONS ON ANTENNAS AND PROPAGATION*, VOL. 54, NO. 2, February 2006.

[5] David M. POZAR & Barry KAUFMAN. (1990). Design Considiration for Low Sidelobe Microstrip Arrays. *IEEE TRANSACTIONS ON ANTENNAS AND PROPAGATION*, VOL. 38, NO. 8, August 1990.

[6] K-L-Wu, M. Spenuk, J. Litva & D. –G Fang. (1991). Theoretical and experimental study of feed network effects on the radiation pattern of series-fed microstrip antenna arrays. *IEE PROCEEDINGS-H,* Vol. 138, No.3, June 1991.

[7] P.S. Hall & C.M. Hall. (1988). Coplanar corporate feed effects in microstrip patch array design. *IEE PROCEEDINGS-H,* Vol. 135, No.3, June 1988.

[8] M.T. Ali, T.A. Rahman, M.R. Kamarudin, M.N. Md Tan and R. Sauleasu. (2009). A Planar Antenna Array with separated feed line for higher gain and sidelobe reduction. *Progress in Electromagnetics Research C*, Vol. 8, 69-82, 2009.

[9] Senhang He, Pu Taug, Bo chen & Pingyou Wang. (2016). Design of an X-band Stripline-fed Co-aperture Microstrip Multilayer Transceiver Array Antenna. *Progress in Electromagnetics Research Symposium*, Shanghai, China, 8-11 August.

[10] Nidheesh Kumar T R, Niraj Kumar, M Sreenivasan, K George Thomas & P H Rao. (2016). A Multilayer X-Band FMCW-SAR Microstrip Array. *IEEE WISPNET 2016 conference*.

[11] Nurulazlina Ramli, Mohd Tarmizi Ali, Mohammad Tariqul Islam, Azita Laily Yusof & Suzilawati Muhamud-Kayat. (2015). Aperture-Coupled Frequency and Pattern reconfigurable microstrip stacked array antenna. *IEEE TRANSACTIONS ON ANTENNAS AND PROPAGATION*, VOL. 63, NO. 3, March 2015.

[12] Hemant Kumar & Girish Kumar. (2016). Microstrip Antenna Array with Ratrace Comparator at X-Band for Monopulse Tracking Radar. *IEEE International Symposium on Antennas and Propagation (APSURSI)*.

[13] Zehn-Guo LIU & Yong-Xin GUO. (2013). Monopulse Fabry-Perot Resonator Antenna. *Proceedings of the International Symposium on Antenna and Propagation (ISAP).*

[14] Zhong-Wu, Guang-Ming Wang & Chen-Xin Zhang. (2009). A Broadband Planar Monopulse Antenna Array of C-Band. *IEEE ANTENNAS AND WIRELESS PROPAGATION LETTERS*, VOL. 8, 2009.

[15] LIN Zheng, LI Wei-ming, XUE Zheng-hui & REN Wu. (2013). Research of Dual-Polarized Monopulse Microstrip Antenna Array. 2013 *IEEE INTERNATIONAL CONFERENCE ON MICROWAVE TECHNOLOGY & COMPUTATIONAL ELECTROMAGNETICS.*

[16] Hai-Yan Huang, Bing-Zhong Wang, Feng Li & Lu Zhao. (2008). A Ka-Band Monopulse Microstrip Antenna Array. *IEEE MTT-S International Microwave Workshop Series on Art of Miniaturizing RF and Microwave Passive components*.

[17] Fengwei Yao, Xiaobo Xuan & Yuanyun Liu. (2013). A Novel Monopulse Edge-fed Microstrip Array Antenna. *5th IEEE International Symposium on Microwave, Antenna, Propagation and EMC Technologies for Wireless Communications.*

[18] Richard C. Johnson (editor). (1993). *Antenna Engineering Handbook.* McGraw-Hill.

[19] Bassem R. Mahafza. (2000*). Radar system Analysis and Design using MATLAB*. Chapman & Hall.

[20] IEEE Antenna and Propagation Society. (2013). *IEEE Standard for definitions of terms for Antenna*, IEEE Xplore.

[21] Ramesh Grag, Prakash Bhartia, Inder Bahl & Apisak lttipiboon. (2001). *Microstrip Antenna design Handbook*. Artech House.

[22] J.R. James & P.S. Hall. (1989). *Handbook of Microstrip Antennas*. Peter Peregrinus.

[23] Constantine A. Balanis. (2005). *Antenna Theory analysis and design*. John Wiley & Sons.

[24] David M. POZAR. (2009). *Microwave engineering*. John Wiley & Sons.

[25] E.H. Fooks & R.A. Zakarevicius. (1990). *Microwave Engineering using Microstrip circuits*. Prentice Hall.

[26] Edgar J. Denlinger. (1980). Losses of microstrip line. *IEEE TRANSACTIONS ON MICROWAVE THEORY AND TECHNIQUES*, VOL. MTT-28, NO. 6, June 1980.

[27] https://www.microwaves101.com/encyclopedias/transmission-line-loss.

[28] Hubregt J. Visser. (2005). *Array and Phased Array Antenna Basics*. John Wiley & Sons.

[29] Fitri Yuli Zulkifli, Taufal Hidayat, Basari & Eko Tjipto Rahardjo. (2013). Sidelobe Level Suppression using Unequal four-way Power devider for Proximity Coupled Microstrip Antenna. *Asia-Pacific Microwave conference Proceedings*.

[30] N.A. Zainal, M.R. Kamarudin, Y. Yamada, Norhudah Seman, Mohsen Khalily & M. Jusoh. (2016). Sidelobe reduction of unequally spaced arrays for 5G Applications. *10th European Conference on Antennas and Propagation (EuCAP)*.

APPENDIX

Appendix A: Ideal Monopulse Pattrens Generation (MATLAB):

```
% Demonstration of the monopulse pattrens
% Allaeldien Hnesh, EMU Fall 2017
clear all
close all
clc
phi=-720:1:720;
phiO=-720:1:720;
for i=1:1:2*720/1+1
phiO(i)=75;
end
for i=1:1:2*720/1+1
B1(i)=sin((phi(i)-phiO(i))*pi/180)/((phi(i)-phiO(i))*pi/180);
B2(i)=sin((phi(i)+phiO(i))*pi/180)/((phi(i)+phiO(i))*pi/180);
sum(i)=B1(i)+B2(i);
diff(i)=B1(i)-B2(i);
end
plot(phi,B1,'red');
xlabel('angle in degree');
ylabel('Pattrens A (red) and B (blue)')
hold, grid
plot(phi,B2);
figure
plot(phi,(sum),'red');
xlabel('angle in degree');
ylabel('Normalized sum (red) and diffrence (blue)')
hold, grid
plot(phi,(diff));
figure
plot(phi,10*log(abs(sum/max(sum))),'red');
xlabel('angle in degree');
ylabel('Normalized sum (red) and diffrence (blue) in dB')
hold, grid
plot(phi,10*log(abs(diff/max(diff))));
```